Advanced Microbiome Therapeutics Accelerate MASLD Recovery by Restoring Intestinal Microbiota Equilibrium and the Gut-Liver Axis in a

JOURNAL OF AGRICULTURAL AND FOOD CHEMISTRY

pubs.acs.org/JAFC
Article

Advanced Microbiome Therapeutics Accelerate MASLD Recovery by Restoring Intestinal Microbiota Equilibrium and the Gut-Liver Axis in a Mouse Model

Johnson Lok,[¶] Congjia Chen,[¶] Valeria Iannone, Ambrin Farizah Babu, Emily Kwun Kwan Lo, Ruben Vazquez-Uribe, Troels Holger Vaaben, Mikko Kettunen, Otto Savolainen, Ursula Schwab, Morten Otto Alexander Sommer, Kati Hanhineva, Marjukka Kolehmainen, Hani El-Nezami,* and Carlos Gómez-Gallego*

Cite This: J. Agric. Food Chem. 2025, 73, 15199−15214

ABSTRACT: Gut microbiota dysbiosis and endocrine dysregulation are key players in metabolic dysfunction-associated steatotic liver disease (MASLD) development. This study evaluated whether advanced microbiome therapeutics can restore intestinal microbial equilibrium and gut-liver axis balance during MASLD recovery. MASLD was induced in mice using a high-fat, high-sugar diet, and then shifted to a standard diet, where intervention groups received engineered *Escherichia coli* Nissle 1917 expressing IGF1 (EcNI) or aldafermin (EcNA), and control groups received *E. coli* Nissle 1917 vehicle (EcN) or no microbial intervention (CTRL). EcNI and EcNA improved MASLD recovery compared to controls by lowering hepatic fat, plasma cholesterol, and body weight, while increasing bacterial diversity, plasma acetate, and propionate, and modulating particular microbial groups, potentially alleviating dysbiosis. Additionally, EcNI and EcNA downregulated acetyl-CoA, the steroid hormone biosynthesis pathway, and EcNA upregulated the pentose phosphate pathway and pyruvate, which are related to oxidative stress reduction. These results suggest that EcNI and EcNA are potential novel treatments for MASLD.

KEYWORDS: *nonalcoholic fatty liver disease (NAFLD), E. coli Nissle 1917, insulin-like growth factor 1, fibroblast growth factor 19, aldafermin, integrative multiomics*

1. INTRODUCTION

Metabolic dysfunction-associated steatotic liver disease (MASLD), previously known as nonalcoholic fatty liver disease (NAFLD), encompasses a range of liver diseases from simple steatosis to metabolic dysfunction-associated steatohepatitis (MASH)[1,2] and hepatocellular carcinoma.[2] Affecting around 30% of the world's population,[3] MASLD's rising global prevalence and progression to severe liver conditions pose a serious public health challenge.[4] Lifestyle changes, including a healthy diet and increased physical activity for weight loss, are the main interventions for MASLD.[5] Weight loss strategies, including dietary interventions, effectively reduce hepatic steatosis and MASLD-related biomarkers,[6,7] and a weight loss goal of over 10% is recommended.[8] However, weight loss is hard to achieve and maintain in lifestyle interventions,[8−10] where less than half of the participants achieved the needed weight loss,[9] and around half could not maintain it beyond one year,[8] possibly influenced by genetic, hormonal, and neural factors.[11] This highlights the need for novel therapeutic approaches to enhance the effectiveness of lifestyle interventions.

The manifestation and progression of MASLD remain poorly understood. The "multiple parallel hits" hypothesis suggests a central role of the gut-liver axis, influenced by factors like diet components, gut microbiota, and metabolic changes.[12,13] Gut microbiota dysbiosis, characterized by reduced microbial diversity, decreased beneficial microbes, and increased potentially harmful microbes,[14] can impair gut barrier functions and increase gut permeability, which is common with MASLD.[13,15−17] This allows proinflammatory microbial metabolites to reach the liver via the hepatic portal vein, exacerbating hepatic inflammation.

There is compelling evidence that hormonal imbalances, notably reduced growth hormone levels, can contribute to MASLD development via several mechanisms.[18,19] Growth hormones primarily stimulate insulin-like growth factor 1 (IGF1) production in the liver. IGF1 can improve hepatic insulin sensitivity[20] and modulate cholesterol transport.[21] IGF1 intervention showed health benefits in individuals and mice with MASLD, MASH, and cirrhosis by reducing steatosis, fibrosis, and inflammation.[20,22,23] Similarly, fibroblast growth factor (FGF) 19 levels are reduced in MASLD.[24] FGF19 is produced in the ileum in response to increased bile acid levels[25] and is involved in bile acid, lipid, and energy

Received: February 7, 2025
Revised: May 12, 2025
Accepted: May 12, 2025
Published: June 6, 2025

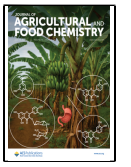

metabolism.[24] Aldafermin, an engineered nontumorigenic analogue of FGF19, showed promise in individuals with MASH by reducing hepatic steatosis.[26]

As impaired hormonal balance and gut microbiome play pivotal roles in MASLD development, we treated MASLD using advanced microbiome therapeutics (AMTs), which are microbes engineered to produce and deliver therapeutics *in situ*.[27] *Escherichia coli* Nissle 1917 was used as the expression platform to produce IGF1 or aldafermin, for restoring hormonal balance. *E. coli* Nissle 1917 was used as a probiotic chassis due to the vast genetic toolbox available for genetic engineering[27,28] and its well-described safety[29] for treating intestinal diseases and delivering various therapeutic molecules.[30] To the best of our knowledge, our study is the first to investigate the use of engineered microbes to express IGF1 and aldafermin for alleviating MASLD.

We hypothesized that the engineered microorganisms could express IGF1 or aldafermin and accelerate the recovery of MASLD by restoring the gut-liver axis balance, which offers a promising new therapeutic possibility for MASLD treatment. We evaluated the effects of AMTs, combined with dietary changes, on alleviating MASLD-related parameters. These include body weight, liver fat accumulation, plasma cholesterol, short-chain fatty acid concentrations, and changes in intestinal microbiota composition and activity.

2. MATERIALS AND METHODS

2.1. Genetic Engineering of *E. coli* Nissle 1917 to Express IGF1 and Aldafermin, Production of Hormones, and Characterization of Bacterial Growth in Strains *In Vitro*. The endogenous pMUT-1-based plasmid was added to *E. coli* Nissle 1917 (Figure S1) and used for stable expression of IGF1 and aldafermin, as previously described.[31] More details are provided in the Supporting Information.

Hormone concentrations in supernatants from bacterial cell cultures grown for 24 h were quantified using enzyme-linked immunosorbent assay (ELISA) kits (Abcam: ab211651 IGF1; ab230943 aldafermin, Cambridge, United Kingdom) according to the manufacturer's protocol. Growth rates were calculated using the cell density change measured with OD600 in the log phase, as previously described.[31] Iannone et al.[31] partly reported the strains' hormone production and growth rate, and new analyses were performed.

2.2. Preparation of Gelatin Cubes with *E. coli* Nissle 1917 Strains for Voluntary Oral Administration. All of the strains were resistant to the antibiotics streptomycin and kanamycin. Bacteria were cultured twice overnight, first in Luria−Bertani (LB) broth containing the two antibiotics and then on LB agar plates without antibiotics. Cells collected in a 10% artificial sweetener ("Hermesetas Crunchy", Zurich, Switzerland) solution were mixed with gelatin in 96-well plates in a 1:1 ratio.[32] Each gelatin cube contained 10^9 colony-forming units (CFUs) of *E. coli* Nissle 1917 and was validated by plating using LB agar plates containing the two antibiotics.

2.3. Animal Study Design. The study was carried out under license ESAVI/21371/2019, approved by the National Ethics Committee for Animal Experiments in Finland, and followed the regulations of the European Union concerning the protection of animals used for scientific purposes and reported in compliance with ARRIVE guidelines.[33] Twenty-four 5- to 8-week-old C57BL/6J male mice bred by the University of Eastern Finland (Kuopio, Finland) animal housing facilities were used. Mice were kept in individually ventilated cages (1−4 mice/cage) under specific-pathogen-free conditions at 20.6 °C (±0.2 °C) and 55% (±0.8%) humidity with a 12/12h light cycle. Power analysis was performed using the "G*Power" program[34] based on data from two previous studies.[35,36] More details are provided in the Supporting Information. To develop MASLD, all mice were given for 14 weeks an ALIOS diet,[37] including a high-fat diet (TD06303, Harlan Teklad, Madison, WI) and drinking water with high-fructose corn syrup equivalent (containing by weight 45% glucose and 55% fructose) at 42 g/L. ALIOS diet-induced MASLD in murine models closely resembles human MASLD progression.[38] After 14 weeks, hepatic steatosis was confirmed using magnetic resonance imaging (MRI). The mice were then randomly assigned to 4 groups (6 mice/group) by drawing lots, and all mice were changed to the standard control diet (2016 Teklad global 16% protein rodent diets, Harlan Teklad, Madison, WI). The intervention mice were conditioned to voluntarily consume gelatin cubes daily[32] for 7 weeks, containing the engineered *E. coli* Nissle 1917 expressing IGF1 (EcNI) or aldafermin (EcNA). Control mice were given gelatin cubes containing *E. coli* Nissle 1917 without expressing hormone (EcN) or vehicle cubes without bacteria (CTRL). Consumption of gelatin cubes was monitored to confirm that all mice received the full intended dose. Data on the histology, body weight, plasma biochemistry, and liver metabolites of mice from EcNA, EcN, and CTRL have been partly published by Iannone et al.,[31] with new analyses performed.

2.4. Magnetic Resonance Imaging. To validate hepatic steatosis after the ALIOS diet intervention and measure the effectiveness of our interventions (Figure S2), MRI was used to quantify the change in liver fat content, as previously described[36] using a 7 T MRI scanner (Pharmascan, Bruker Biospin, Ettlingen, Germany) with a quadrature volume coil transmitter and a quadrature rat head surface coil receiver (Rapid Biomedical, Rimpar, Germany).

2.5. Sample Collection. Body weight was measured weekly and on the day of sacrifice. The concentration of viable *E. coli* Nissle 1917 in EcN, EcNI, and EcNA mice was quantified as CFUs/g of fecal samples collected the day before mice sacrifice *via* plating on LB agar with antibiotics. On the day of sacrifice, the mice were fasted for 2 h to minimize variability in physiological and biochemical parameters.[39] They were then administered terminal anesthesia with pentobarbital (Mebunat vet, Orion Pharma, Espoo, Finland) *via* intraperitoneal injection starting at 2 mL/kg of body weight until a negative pedal reflex was observed. Blood was extracted *via* cardiac puncture, and plasma was isolated using BD Microtainer blood collection tubes (Category number: 365986, Becton, Dickinson and Company, Franklin Lakes, NJ). Cardiac perfusion was carried out immediately after blood extraction. The liver was weighed before being processed for histology. Plasma, colon, and cecum contents were snap-frozen in liquid nitrogen before being stored at −80 °C.

2.6. Plasma Biochemistry and Hormone Concentrations. Plasma samples were diluted with 0.9% NaCl in a 1:3 ratio. Concentrations of aspartate aminotransferase, alanine aminotransferase, high-density lipoprotein (HDL), low-density lipoprotein (LDL), total cholesterol, triglycerides, and glucose were determined using an automated clinical chemistry analyzer Konelab Prime 60 (Thermo Fisher Scientific, Waltham, MA). Concentrations of IGF1 and aldafermin in undiluted plasma were quantified using the same ELISA kits, as described in Section 2.2.

2.7. Short-Chain Fatty Acid (SCFA) Analysis in Plasma and Cecum Content. Samples (10 μL of plasma, feces ∼20 mg/mL dissolved in ultrapure Milli-Q water) were incubated with 75% methanol (MeOH) (60 μL), 3-NPH (10 μL; 200 mM in 75% MeOH), and EDC-6% pyridine (10 μL; 120 mM in MeOH) at ambient temperature for 45 min, while shaking in a dvx-2500 multitube vortexer (VWR) at 1600 rpm. The reaction was quenched by adding quinic acid (10 μL; 200 mM in 75% MeOH), followed by vortex shaking at 1600 rpm for 15 min and centrifugation at 15 000 g for 5 min. The supernatant was collected, made up to 1 mL using 10% MeOH in water, and again centrifuged at 15,000*g* for 5 min. An aliquot of the derivatized sample (100 μL) was mixed with an equal volume (100 μL) of the labeled (13C6−3NPH) internal standard mix prior to analysis by targeted ultrahigh-performance liquid chromatography coupled to tandem mass spectrometry (UHPLC-MS/MS). UHPLC-MS/MS analytics of SCFA was conducted, as previously reported by Fristedt et al.[40] More details are provided in the Supporting Information.

https://doi.org/10.1021/acs.jafc.5c01674
J. Agric. Food Chem. 2025, 73, 15199−15214

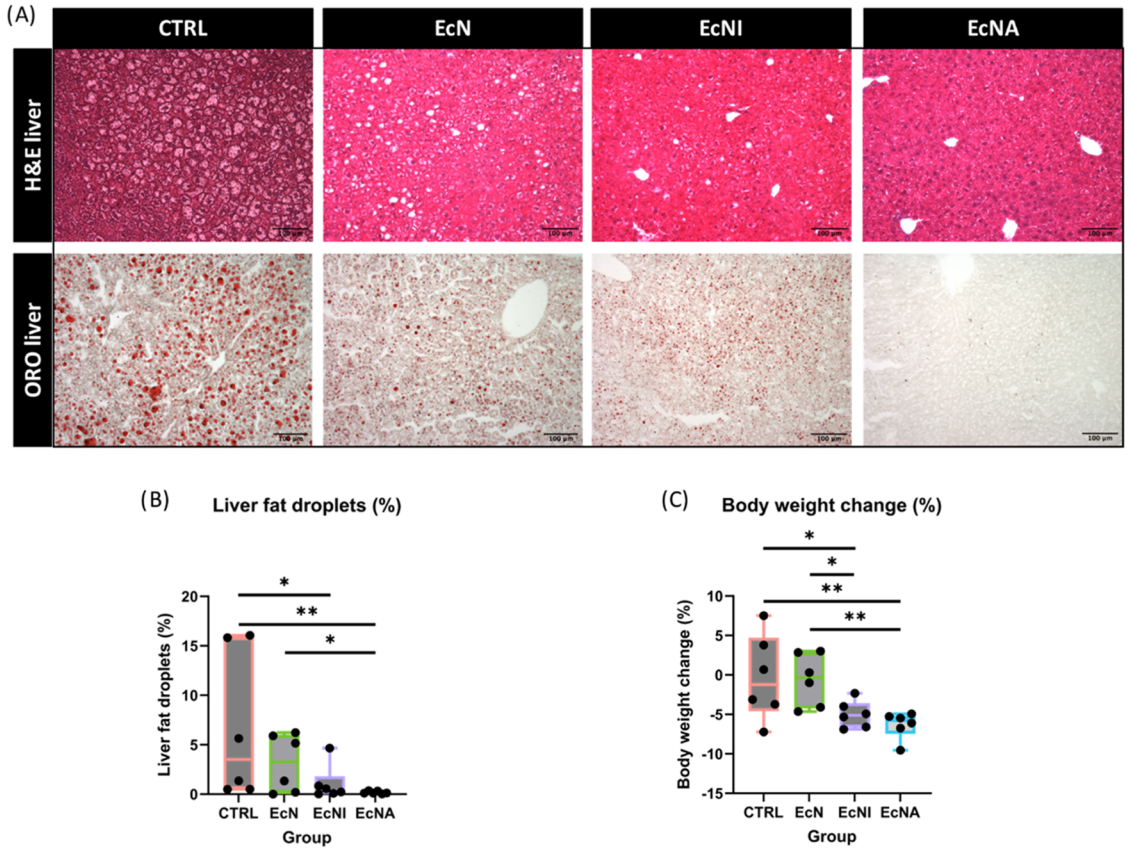

Figure 1. EcNI and EcNA alleviated several MASLD-related parameters. (A) Representative pictures of liver histology stained using H&E and ORO (H&E staining: $n = 6$ mice/group, scale bar 100 μm, 10× objective. ORO staining, stained fat droplets appear as red dots: $n = 6$ mice/group, scale bar 100 μm, 10× objective). Boxplots of (B) percentage of liver fat droplets quantified by ORO staining ($n = 6$ mice/group, 8 acquisitions/mouse) and (C) percentage of body weight change ($n = 6$ mice/group). Statistical significance between groups is indicated by asterisks (* $p \leq 0.05$, ** $p \leq 0.01$). H&E: hematoxylin and eosin; ORO: Oil Red O.

Formic, acetic, propionic, butyric, isobutyric, succinic, valeric, isovaleric, and caproic acid concentrations were obtained by normalizing each analyte response with the respective 13C6−3NPH isotopically labeled internal standard and then calibration with external calibration curves. The total SCFA concentration was calculated by summing the values of all individual SCFAs, where samples with any missing SCFA values were excluded.

2.8. Liver Histology. Liver samples from the left lateral lobe were collected for histology, as previously described.[36] In short, liver processed and embedded into paraffin blocks was used for hematoxylin (Bio-Optica, Milan, Italy) and eosin (Bio-Optica, Milan, Italy) staining, while frozen liver samples were used for Oil Red O (ORO; Sigma-Aldrich, Saint Louis, MO) staining. Histological images were captured using a BX51 microscope (Olympus, Tokyo, Japan). The percentage of liver fat droplets in the sections stained with ORO was measured using Fiji (ImageJ) software (version 1.52p) with trainable Weka Segmentation plugin.[41]

2.9. 16S and Internal Transcribed Spacer (ITS) rRNA (rRNA) Sequencing. DNA was extracted from the cecum content using the QIAamp PowerFecal Pro DNA Kit (Qiagen, Germany) according to the manufacturer's instructions. Before bead beating, a heating step of 65 °C for 10 min followed by an enzymatic digestion step with 3 μL of mutanolysin (10 U/mL; Sigma-Aldrich), 6 μL of lysozyme (20 mg/mL; Sigma-Aldrich, Canada), and 5 μL of lyticase (1500 U/mL; Sigma-Aldrich, Japan) per sample at 37 °C for 60 min were performed. Extracted genomic DNA was quantified using a Qubit dsDNA BR Assay Kit (Thermo Scientific, Waltham, MA) with a Qubit 4.0 fluorometer (Thermo Scientific, Waltham, MA). Quality was assessed based on the A260/A280 ratio using a NanoDrop ND-1000 Spectrophotometer (NanoDrop Technologies, Wilmington, DE). 16S and ITS rRNA sequencing using the NovaSeq 6000 sequencing platform was purchased as a service from Novogene Co., Ltd. (Beijing, China). More details are provided in the Supporting Information.

2.10. Nontargeted Metabolomics Analysis. The method developed by Klåvus et al.[42] was followed for nontargeted metabolomics analysis. Briefly, the liver, colon, and cecum contents were homogenized in 80% methanol, vortexed, centrifuged, and the supernatant was collected. After thawing on ice and vortexing, 50 μL of plasma was mixed with 200 μL of cold acetonitrile (VWR). The supernatants and processed plasma samples were then filtered (Captiva ND filter plate 0.2 μm) by centrifugation for 5 min at 4 °C and 700g and kept at 4 °C until analysis. Reversed-phase liquid chromatography (LC) using a Vanquish Flex UHPLC 238 system (Thermo Scientific, Bremen, Germany) coupled to high-resolution Orbitrap mass 239 spectrometer (Q Exactive Focus, Thermo Scientific, Bremen, Germany), and hydrophilic interaction LC on 1290 Infinity Binary UPLC coupled with a 6540 UHD Accurate-Mass quadrupole 243 time-of-flight MS (Agilent Technologies, California, United States) were conducted, where both positive and negative electrospray ionization modes were used for data collection, as previously described.[36] More details are provided in the Supporting Information.

2.11. Statistical Methods and Comparisons. Statistical analyses on hormone concentration and growth rate of *E. coli* strains, body weight, MRI fat index, liver weight, and viable *E. coli* CFUs, liver fat content measured with MRI, plasma biochemical parameters, SCFA concentrations, liver fat droplets measured with histology, and CAG representative values were conducted using the Kruskal−Wallis test followed by Dunn's posthoc tests to identify significant differences among the groups and the specific group differences. All statistical analyses were performed using R software (version 4.3.0)[43]

https://doi.org/10.1021/acs.jafc.5c01674
J. Agric. Food Chem. 2025, 73, 15199−15214

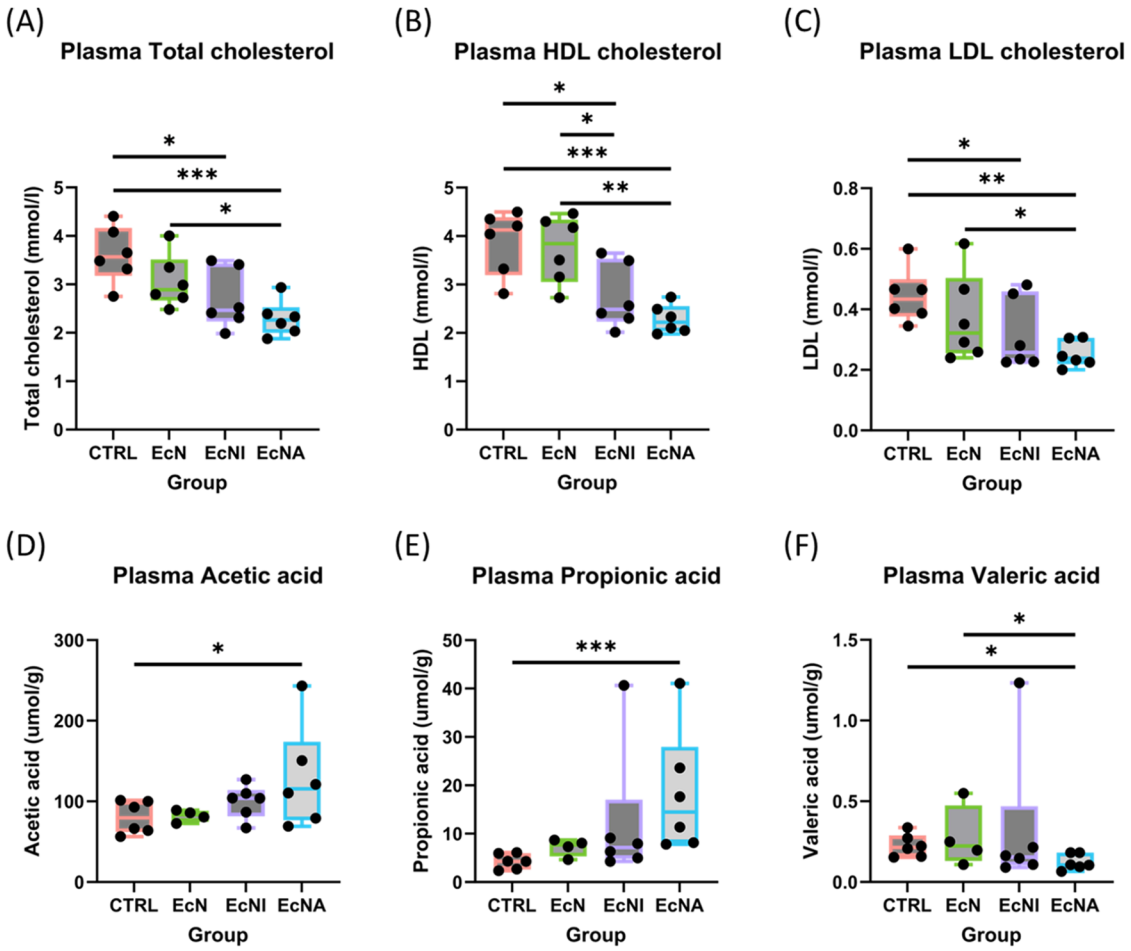

Figure 2. EcNI and EcNA reduced plasma cholesterol and increased plasma SCFA concentrations. Boxplots of plasma (A) total cholesterol (n = 6 mice/group), (B) HDL cholesterol (n = 6 mice/group), (C) LDL cholesterol (n = 6 mice/group), (D) acetic acid (n = 4−6 mice/group), (E) propionic acid (n = 4−6 mice/group), and (F) valeric acid (n = 4−6 mice/group) concentrations. Statistical significance between groups is indicated by asterisks (* $p \leq 0.05$, ** $p \leq 0.01$, *** $p \leq 0.001$). SCFA: short-chain fatty acid; HDL: high-density lipoprotein; LDL: low-density lipoprotein.

and visualized using Box and Whisker diagrams with GraphPad Prism version 10.0.3 for Windows, GraphPad Software (Boston, MA, www.graphpad.com). More details on the statistical analyses of 16S and ITS rRNA sequencing and metabolomics data are provided in the Supporting Information.

3. RESULTS

3.1. Engineered *E. coli* Nissle 1917 Produced IGF1 and Aldafermin *In Vitro* and Survived Gut Transit *In Vivo*. The strains produced *in vitro* IGF1 at 659 ± 60.7 ng/mL/OD600 and aldafermin at 12.7 ± 1.46 ng/mL/OD600 (Figure S3A). However, the levels of aldafermin and IGF1 in the systemic blood samples of the mice included in this study were below the detection limits of the ELISA kits used for quantification. Expression of IGF1 did not significantly affect the strain's growth rate, which is a proxy measurement of cell fitness (Figure S3B). However, overexpression of aldafermin resulted in a 55% reduction in the growth rate (Figure S3B) compared to the *E. coli* Nissle 1917 vehicle without hormone expression.

Toward the end of the *in vivo* mouse intervention, viable *E. coli* Nissle 1917 were recovered using agar plating from mice receiving *E. coli* intervention. The concentration of viable *E. coli* recovered was 10^4 to 10^6 colony-forming units (CFUs) per gram of feces (Figure S3C). The impaired growth rate of the strain expressing aldafermin (Figure S3B) could hamper its ability to persist in the gut, which was also reflected in the decrease in viable counts (Figure S3C). However, such a decrease was not statistically significant. These results showed that all tested strains temporarily colonized and survived the whole gastrointestinal transit.

3.2. EcNI and EcNA Reduced Liver Steatosis, Body Weight, Plasma Cholesterol, and Changed SCFAs. Combined with dietary changes, mice underwent interventions with *E. coli* Nissle 1917 expressing IGF1 (EcNI) or aldafermin (EcNA) alleviated several MASLD-related parameters more effectively than the control with dietary change alone (CTRL) or with added *E. coli* Nissle 1917 vehicle (EcN). The EcNI and EcNA groups had lower hepatic steatosis. Hematoxylin and eosin (H&E) staining showed that the liver morphology was well preserved with little to no observable fat lipid droplets in EcNA and, to a lesser extent, in EcNI compared to the control groups (Figure 1A). Quantifying the Oil Red O (ORO) staining results further showed that hepatic steatosis in the EcNI and EcNA groups was lower than that in the control groups ($p < 0.05$).

EcNI and EcNA consistently resulted in greater body weight loss compared to CTRL and EcN ($p < 0.05$ for all comparisons; Figures 1C and S4) and lower plasma total,

https://doi.org/10.1021/acs.jafc.5c01674
J. Agric. Food Chem. 2025, 73, 15199−15214

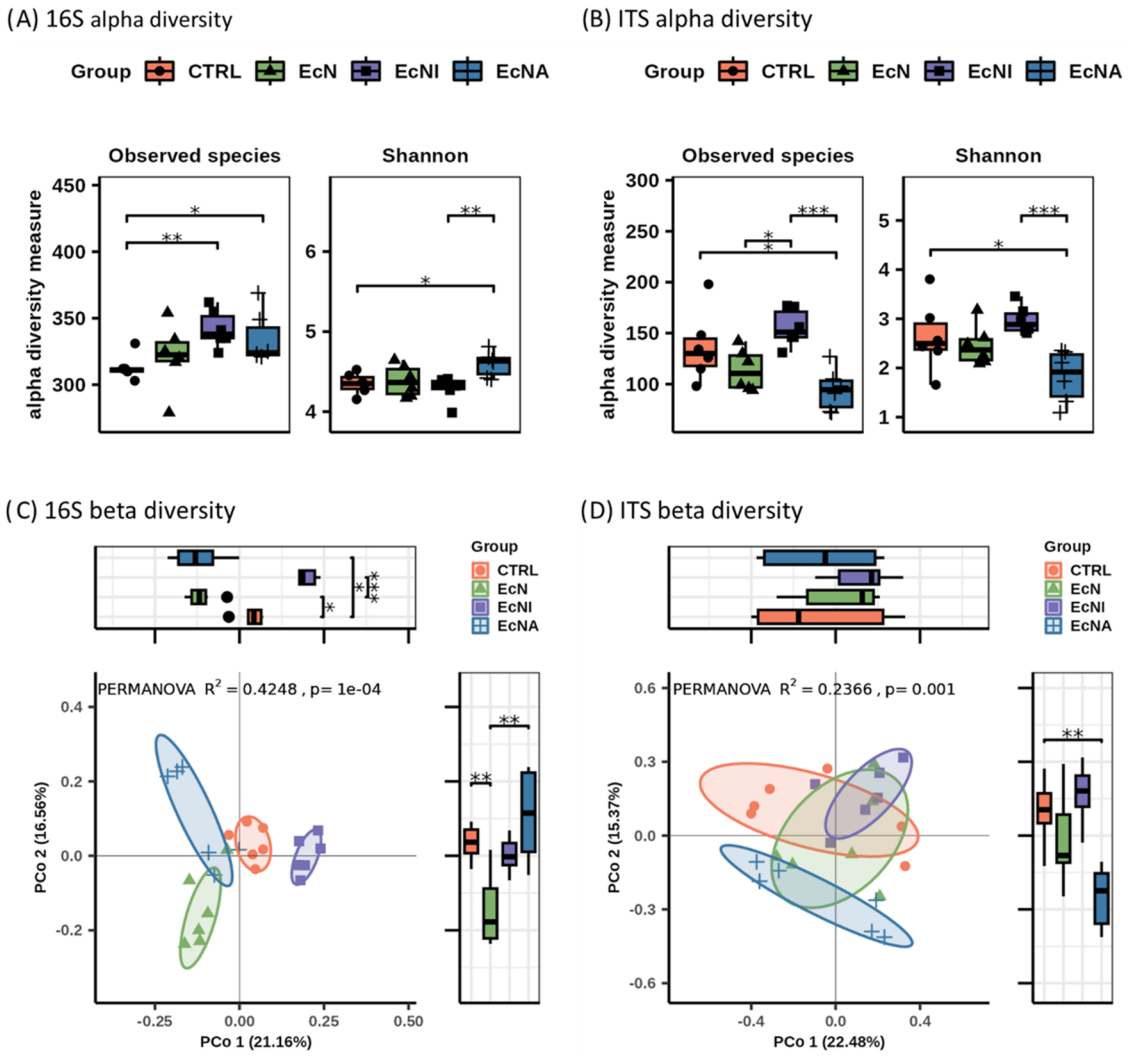

Figure 3. EcNI and EcNA shifted the cecal microbial composition. Boxplots showing the distribution of α diversity measure at the ASV level, including observed species richness and Shannon index of microbial communities in (A) 16S and (B) ITS (n = 6 mice/group). Principal coordinate analysis (PCoA) of microbial communities from (C) 16S and (D) ITS based on the Bray−Curtis distance matrix at the ASV level (n = 6 mice/group). Boxplots along the axes of PCoA displayed the distributions and quartiles of PCo1 (top) and PCo2 (right). Statistical significance between groups is indicated by asterisks (* $p \leq 0.05$, ** $p \leq 0.01$, *** $p \leq 0.001$). PCo: principal coordinate.

high-density lipoprotein (HDL), and low-density lipoprotein (LDL) cholesterol concentrations compared to CTRL ($p < 0.05$ for all comparisons; Figure 2A−C).

SCFA concentrations in the plasma and cecum contents were measured (Table S1). EcNA had significantly higher concentrations of plasma acetic acid and propionic acid than CTRL and a lower concentration of plasma valeric acid than CTRL and EcN ($p < 0.05$ for all comparisons) (Figure 2D−F).

3.3. EcNI and EcNA Modulated Cecal Gut Microbial Composition and Increased Bacterial Diversity. The effects of EcNI and EcNA on cecal gut microbiota were investigated with 16S rRNA sequencing for bacteria and ITS rRNA sequencing for fungi. There were 645 amplicon sequence variants (ASVs) and 148 genera from 16S, and 452 ASVs and 42 genera from ITS were identified. Regarding bacterial composition, compared to CTRL, EcNI had higher ASV richness, measured as observed species, while EcNA had greater ASV richness and Shannon index (all $p < 0.05$) (Figure 3A). For the β diversity analysis, there was a distinct clustering pattern of bacterial composition between groups ($p < 0.05$; Figure 3C). The principal coordinate analysis (PCoA) scatter plot showed that EcN was closer to EcNA than EcNI, indicating that EcNI had a more distinct bacterial profile than EcNA compared with EcN. Regarding fungal composition, EcNA had a lower ASV richness and Shannon index (both $p < 0.05$) than CTRL (Figure 3B). For the β diversity analysis, EcNI was significantly different from CTRL, while EcNA was significantly different from EcN and EcNI ($p < 0.05$) (Figure 3D).

For bacterial genera, compared to CTRL, EcNI had higher abundances of *Akkermansia*, *Eubacterium* J (a polyphyletic group with representative species being *Eubacterium plexicaudatum* in the present study), and *Faecalibaculum*, while the abundance of *Bacteroides* H (a polyphyletic group with representative species being *Bacteroides helcogenes* and *Bacteroides acidifaciens*) was lower (Figure 4). EcNA had significantly higher abundances of *Eubacterium* J, and lower abundances of *Faecalibaculum* than CTRL. Regarding fungal genera, both EcN and EcNA had lower abundances of *Talaromyces* than CTRL (Figure 4).

To investigate the beneficial effects of EcNI and EcNA on the gut-liver axis, partial Spearman correlation was used to

https://doi.org/10.1021/acs.jafc.5c01674
J. Agric. Food Chem. 2025, 73, 15199−15214

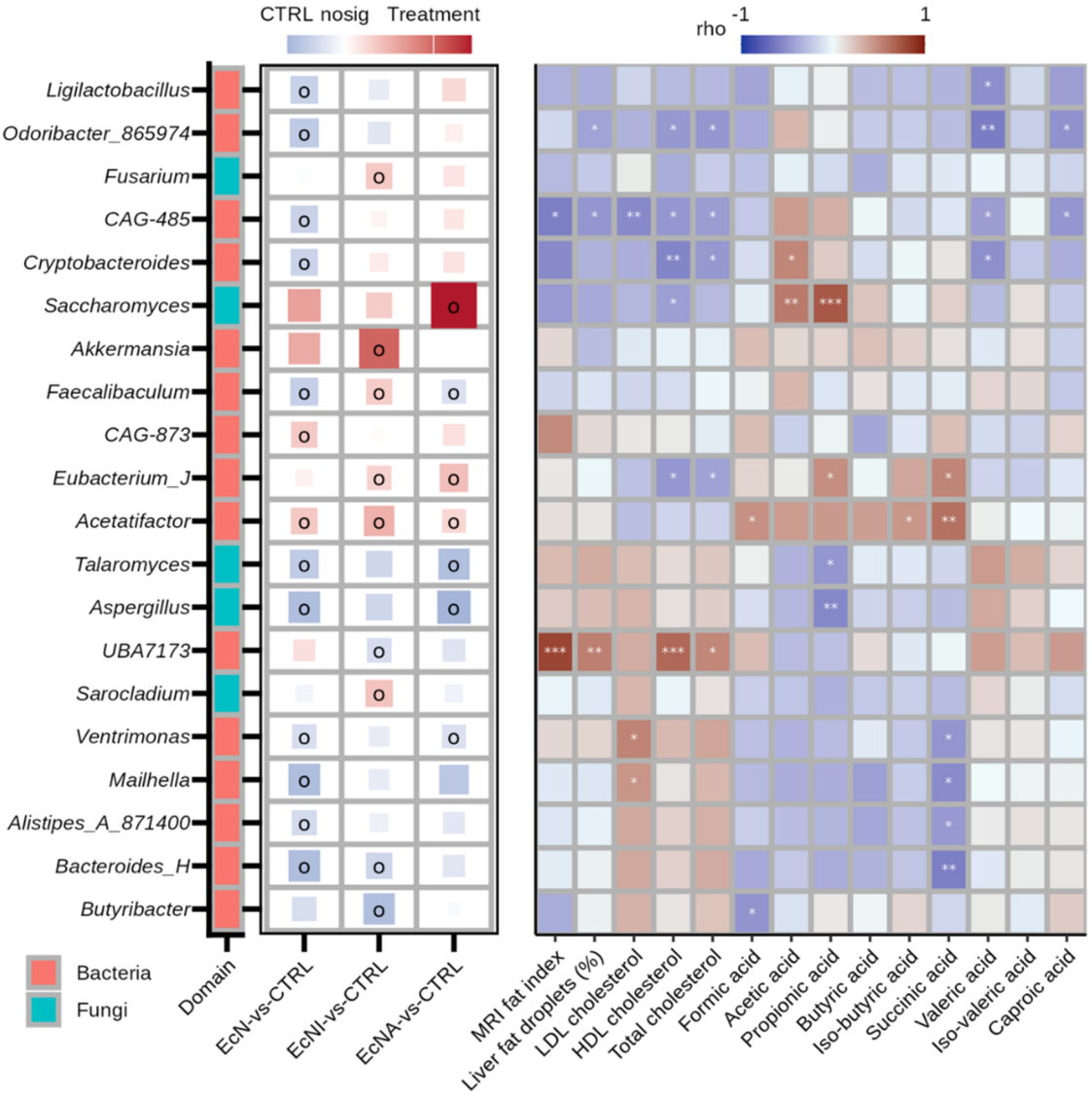

Figure 4. EcNI and EcNA altered the abundance of specific microbial genera and their correlation with MASLD-related parameters. Differential abundant genera based on ANCOM-BC and LDA scores are displayed in the left panel (n = 6 mice/group). The color is proportional to log2-transformed fold change, indicating whether the genera have higher abundance in mice without treatment (CTRL, blue) or mice with microbial treatments EcN/EcNA/EcNI (Treatment, red), while size is proportional to the absolute value of log2-transformed fold change. The genera labeled with circles represent adjusted p-value <0.05, fold change >2 or <1/2, and LDA score >3 in each comparison. Each genus is labeled with its corresponding domain. Heatmap showing the partial Spearman correlation between differential organisms' abundance and liver disease-related parameters, plasma cholesterol concentrations, and SCFA concentrations after controlling for the body weights is displayed in the right panel. The color and size of the square are proportional to Spearman's rank correlation coefficient rho (r_s). Statistical significance between groups is indicated by asterisks (* $p \leq 0.05$, ** $p \leq 0.01$, *** $p \leq 0.001$). ANCOM-BC: analysis of compositions of microbiomes with bias correction; LDA: linear discriminant analysis; MRI: magnetic resonance imaging; LDL: low-density lipoprotein; HDL: high-density lipoprotein; SCFA: short-chain fatty acids.

associate the genera with MASLD-associated parameters, plasma cholesterol, and SCFA concentrations. *Eubacterium* J, higher in both EcNI and EcNA compared to CTRL, had significantly negative correlations with plasma HDL cholesterol ($r_s = -0.472$, $p < 0.05$) and total cholesterol ($r_s = -0.420$, $p < 0.05$), and positive correlations with plasma SCFAs propionic acid ($r_s = 0.477$, $p < 0.05$) and succinic acid ($r_s = 0.519$, $p < 0.05$). Furthermore, liver fat droplets were strongly negatively correlated with plasma propionic acid ($r_s = -0.611$, $p < 0.05$), and strongly positively correlated with plasma valeric acid ($r_s = 0.559$, $p < 0.05$) (Figure S5), indicating a potential role in the treatments played in liver fat accumulation *via* SCFAs. Additionally, *Bacteroides* H, which was lower in EcNI and EcN than in CTRL, was negatively correlated with plasma succinic acid ($r_s = -0.598$, $p < 0.05$). The fungal *Talaromyces*, which was lower in EcNA than in CTRL, correlated negatively with plasma propionic acid ($r_s = -0.479$, $p < 0.05$). Overall, these findings indicate that EcNI and EcNA affected microbiota composition and metabolic activity.

3.4. EcNI and EcNA Groups Showed Distinct Metabolic Patterns Compared to the Control Groups EcN and CTRL. To discriminate global metabolic composition across groups, data trends were identified using partial least-squares discriminant analysis (PLS-DA) (Figure 5A). In all four sample types, EcN, EcNI, and EcNA presented a clear separation of metabolite composition relative to CTRL,

https://doi.org/10.1021/acs.jafc.5c01674
J. Agric. Food Chem. 2025, 73, 15199−15214

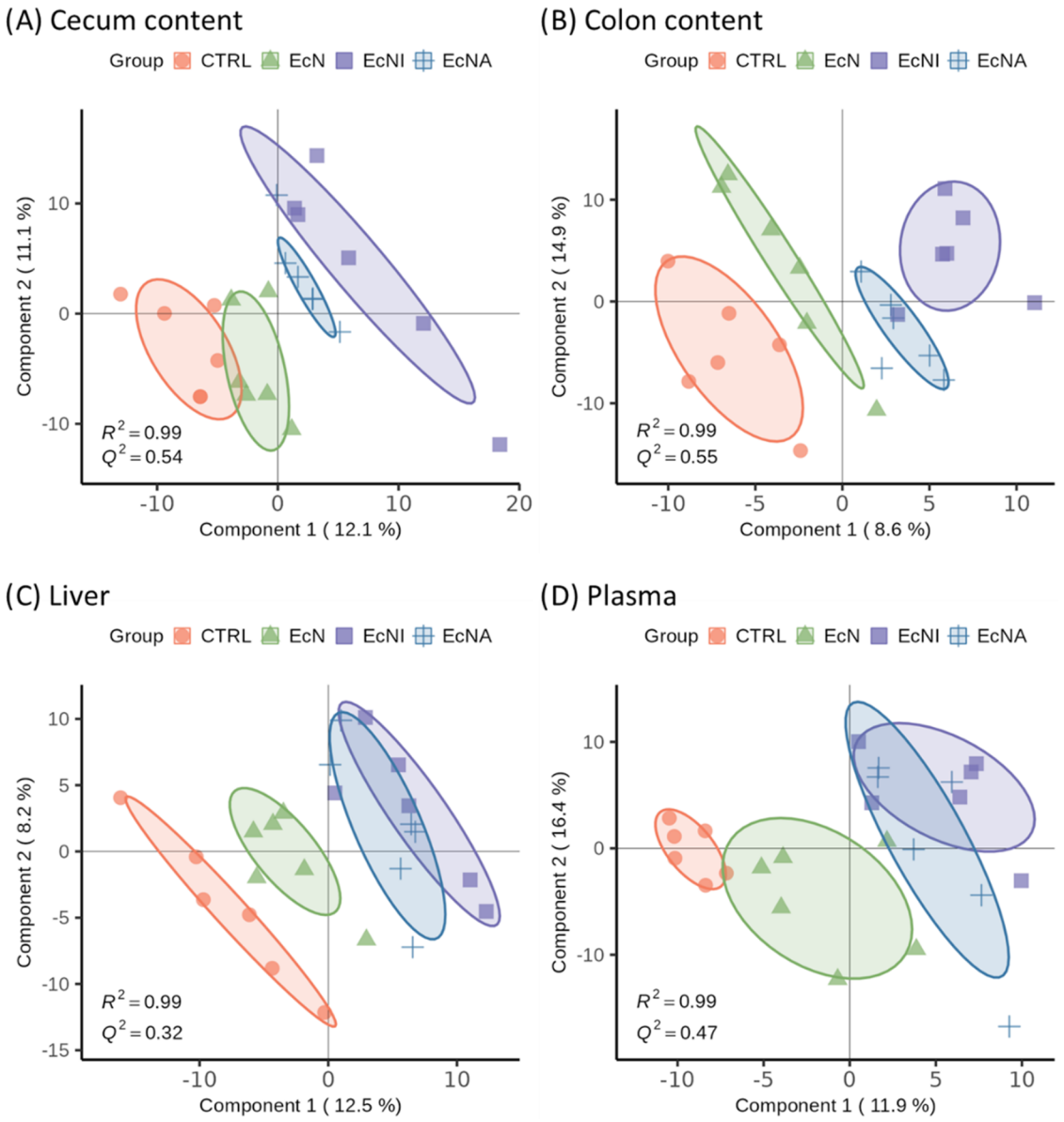

Figure 5. Differential clustering of different intervention groups based on the metabolic patterns in various sample types. PLS-DA score plots based on metabolic profiles in (A) cecum content, (B) colon content, (C) liver, and (D) plasma samples from different intervention groups (n = 6 mice/group). R^2 (coefficient of determination) and Q^2 (predictive ability) were used to validate the model based on 5-fold cross-validation. PLS-DA: partial least squares discriminant analysis.

particularly in the cecum and colon contents (Figure 5A–D). In all four PLS-DA scatter plots, CTRL was closer to EcN than EcNI and EcNA, suggesting that EcNI and EcNA have more distinct metabolic profiles than EcN compared to CTRL.

3.5. EcNI and EcNA Regulated Potential Host-Bacteria Cometabolism Functions through the Gut-Liver Axis. Compared to CTRL, for lipid-related pathways, EcNI had a lower abundance of metabolites involved in the steroid hormone biosynthesis pathway in plasma and a higher abundance of metabolites involved in steroid biosynthesis in colon content (Figures 6A, S6 and S7). For carbon-related pathways, EcNI had a higher abundance of metabolites involved in pyruvate metabolism in the liver than in CTRL. Liver fat droplets were negatively associated with the metabolites involved in the pathways upregulated in EcNI, while they were positively associated with those downregulated in EcNI in the corresponding sample types. Furthermore, the steroid hormone biosynthesis pathway, which positively correlated with liver fat droplets in plasma, was consistently depleted from plasma metabolites and bacterial metabolism in EcNI. Additionally, the steroid biosynthesis pathway with upregulated colon content metabolites and bacterial metabolism in EcNI compared to CTRL was negatively correlated with liver fat droplets (Figure 6A).

The majority of pathways with metabolites lower in EcNA compared to CTRL were lipid-related signaling metabolism pathways, including steroid hormone biosynthesis in plasma (Figures 6B and S8–S15). These pathways were also positively associated with liver fat droplets, indicating that EcNA may regulate host energy homeostasis and lipid metabolite signaling. In contrast, metabolites in carbohydrate-related pathways were higher in EcNA than CTRL, including glycolysis or gluconeogenesis, pentose phosphate pathway in cecum content, glycolysis or gluconeogenesis, citrate cycle,

https://doi.org/10.1021/acs.jafc.5c01674
J. Agric. Food Chem. 2025, 73, 15199–15214

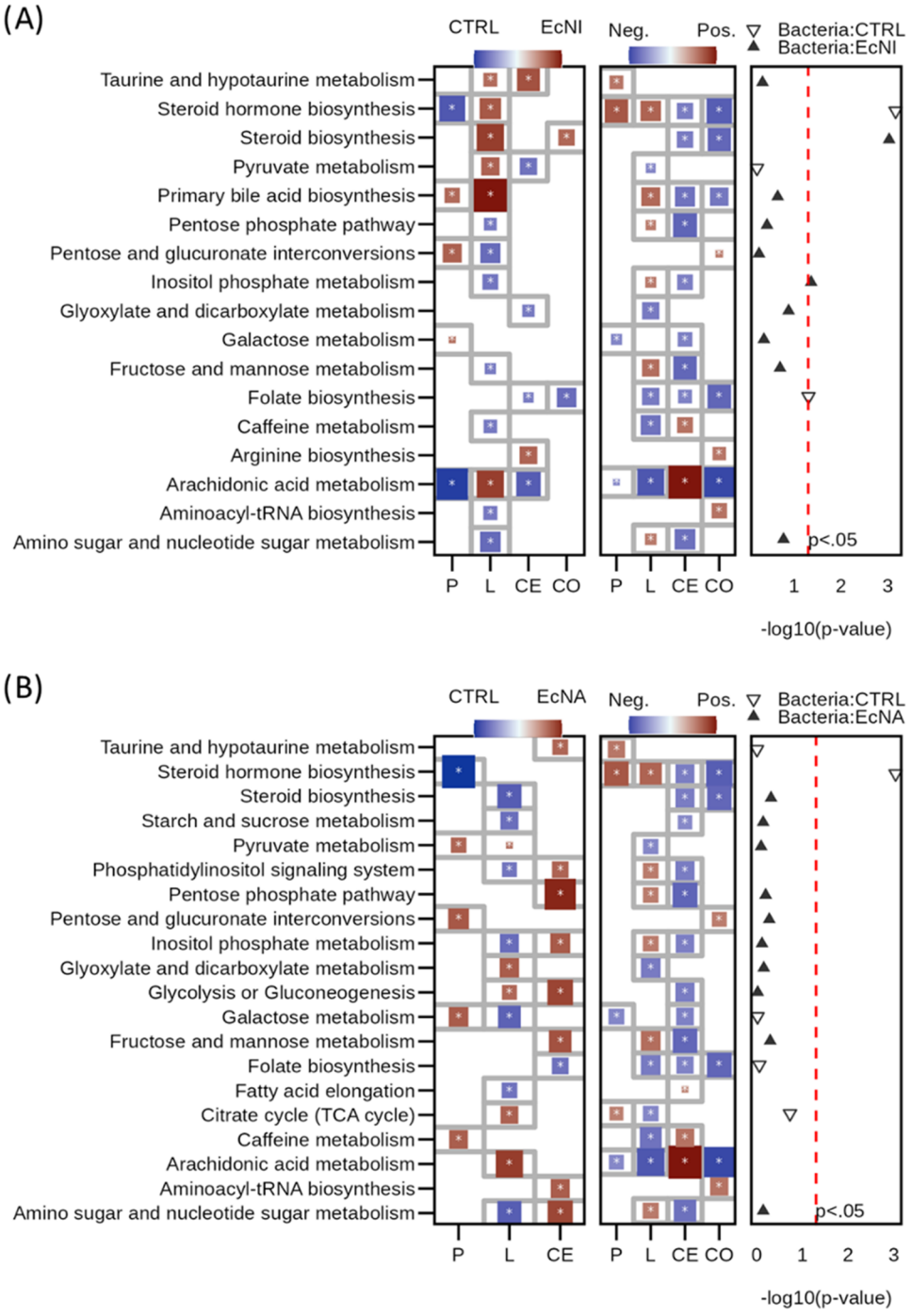

Figure 6. Functional insights from KEGG pathways modulated by EcNI and EcNA. The left heatmap displays the host metabolic KEGG pathway relating to groups with and without microbial interventions in different sample types, based on Gene set enrichment analysis (GSEA) employed in the R package MetaboAnalystR (n = 6 mice/group). The color is proportional to the normalized enrichment score (NES), indicating whether the metabolite sets/pathway is enriched in CTRL (blue) or in the group with microbial intervention (red), including (A) EcNI and (B) EcNA, while size is proportional to the absolute value of NES. The middle plot displays the association between liver fat droplets (%) and host metabolic KEGG pathway, similarly based on gene set enrichment analysis (GSEA) employed in the R package MetaboAnalystR. The right plot displays the differential analysis of the bacteria KEGG pathway estimated by picrust2, whereas the shape represents which group the bacteria KEGG pathway is enriched in. Statistical significance is indicated by asterisks (*$p \leq 0.05$). KEGG: Kyoto Encyclopedia of Genes and Genomes; Neg: negatively associated; Pos: positively associated; CE: cecum content; CO: colon content; L: liver; P: plasma; TCA: tricarboxylic acid; tRNA: transfer ribonucleic acid; PICRUSt2: Phylogenetic Investigation of Communities by Reconstruction of Unobserved States 2.

glyoxylate and dicarboxylate, pyruvate metabolism in the liver, and pyruvate metabolism in plasma. All of these pathways, except the glycolysis or gluconeogenesis pathway in the liver, were also negatively associated with liver fat droplets in the corresponding sample types, implying that EcNA may regulate energy homeostasis and carbohydrate metabolism to alleviate liver fat accumulation (Figure 6B). Notably, we observed that the steroid hormone biosynthesis pathway, which was

https://doi.org/10.1021/acs.jafc.5c01674
J. Agric. Food Chem. 2025, 73, 15199−15214

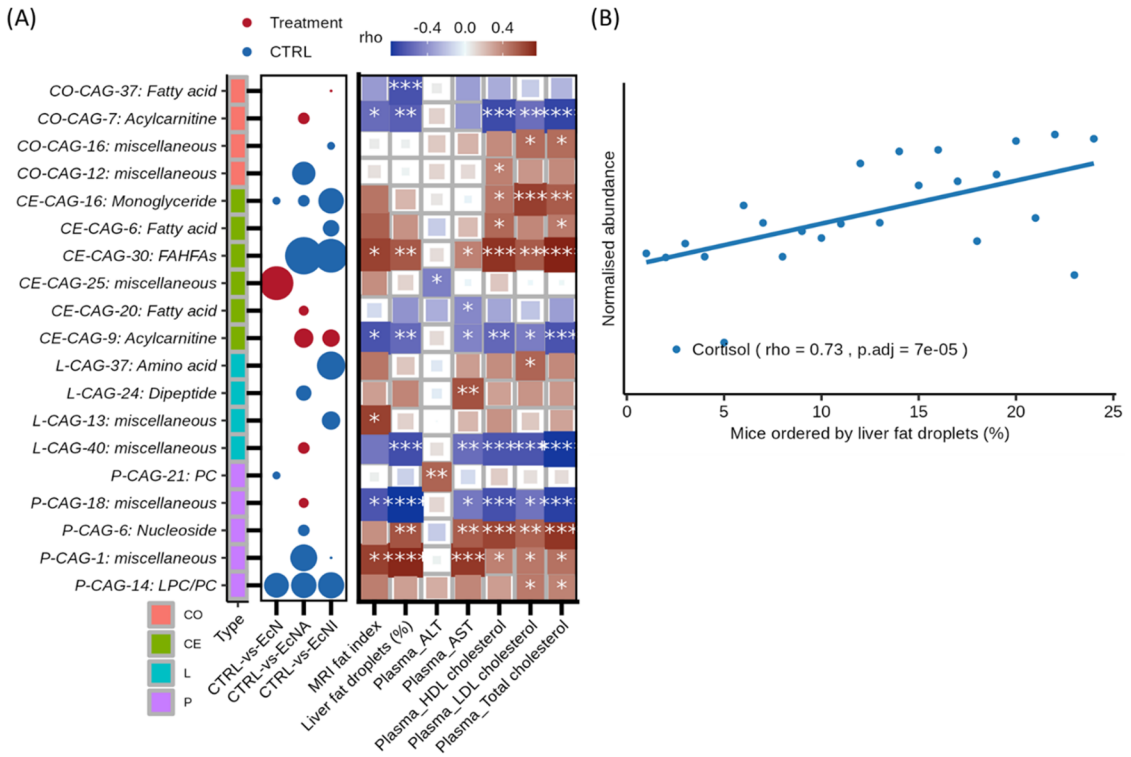

Figure 7. Functional insights from coabundance groups (CAGs) of metabolites modulated by EcNI and EcNA. (A) Metabolite coabundance groups (CAGs) are associated with liver disease indicators and metabolic biomarkers. Metabolite CAGs were calculated using the WGCNA algorithm. The category names for CAGs were determined on the basis of the most abundant metabolites in the CAGs. Further details are provided in Table S2. The left bubble plot shows whether the CAGs have significant differences between different groups. Differential analysis was conducted using the Kruskal−Wallis test followed by Dunn's posthoc test. The size of the bubble is proportional to the $-\log_{10}$-transformed p values. The right heatmap displays the Spearman's association between CAGs, liver disease indicators, and other metabolic biomarkers after adjusting for the effect of body weight. (B) The steroid hormone cortisol shows a strong positive correlation with liver fat droplets in plasma. The scatter plot displays the relationship between the normalized abundance of cortisol (y-axis) and the rank order of mice based on the liver fat droplet percentage (x-axis). CE: cecum content; CO: colon content; L: liver; P: plasma; FAHFA: fatty acyl esters of hydroxy fatty acid; PC: phosphatidylcholine; LPC: lysophosphatidylcholine; MRI: magnetic resonance imaging; ALT: alanine aminotransferase; AST: aspartate aminotransferase; HDL: high-density lipoprotein; LDL: low-density lipoprotein.

positively correlated with liver fat droplets, was downregulated in both plasma metabolites and bacterial metabolism in EcNA relative to CTRL (Figures 6B and S15), highlighting the potential role of EcNA intervention in regulating the interplay between host and bacterial metabolism.

3.6. EcNI and EcNA Modulated Clusters of Metabolites in the Gut-Liver Axis. To overcome the annotation challenge and low pathway completeness, the metabolites from the four sample types were summarized into coabundance groups (CAGs) based on highly correlated abundance patterns across samples (Figure 7A). Metabolites within the same CAG are assumed to be functionally related or coregulated. From the metabolites in the colon and cecum content, liver, and plasma, 4, 6, 4, and 5 CAGs were identified, respectively. Compared to CTRL, seven of these CAGs were higher in our treatment groups and, in general, were negatively correlated with MASLD-related parameters. On the other hand, 12 of these CAGs were higher in CTRL and positively correlated with MASLD-related parameters. Specifically, relative to CTRL, EcNI and EcNA had a higher abundance of miscellaneous P-CAG-1 in the plasma ($p < 0.05$, Figure 7A). Miscellaneous P-CAG-1, including a member of the steroid hormone cortisol, displayed a strong significant correlation with liver fat droplets ($r_s = 0.73$, $p < 0.05$, Figure 7A). In particular, there was a significant positive association between liver fat droplets and the steroid hormone cortisol in the plasma, which was also involved in the KEGG steroid hormone production pathway ($r_s = 0.73$, $p < 0.05$, Figure 7B).

4. DISCUSSION

In this study, we investigated the effects of advanced microbiome therapeutics (AMTs) in MASLD in combination with dietary changes using *E. coli* Nissle 1917 genetically engineered to express IGF1 (EcNI) or aldafermin (EcNA). We have previously demonstrated the beneficial effects of EcNA in the liver by reducing hepatic steatosis and possibly reducing oxidative stress and insulin resistance,[31] and in epididymal visceral adipose tissue by possibly improving insulin sensitivity and energy metabolism[44] in the MASLD mouse model. In this work, we demonstrated that both EcNI and EcNA modulated the gut microbiota and metabolomic profiles in the liver, plasma, colon content, and cecum content along the gut-liver axis to enhance the recovery of MASLD.

The EcNI and EcNA intervention groups had significantly lower body weight, hepatic steatosis, and plasma total, HDL, and LDL cholesterol concentrations than the CTRL and EcN control groups. CTRL exhibited a more heterogeneous and inconsistent response, especially with regard to body weight and hepatic steatosis. Some CTRL mice had low hepatic steatosis and reduced body weight after the intervention, while

https://doi.org/10.1021/acs.jafc.5c01674
J. Agric. Food Chem. 2025, 73, 15199−15214

others had high hepatic steatosis and gained body weight. This is consistent with observations from clinical trials, where not all participants responded well to lifestyle interventions, including dietary change.[8−10] These results support the use of AMTs producing IGF1 and aldafermin, which were more effective in improving the MASLD condition than dietary change alone.

EcNI and EcNA elicited distinct modulating effects on gut microbiota composition, resulting in differentiated microbial communities among the groups. Compared to CTRL, EcNI and EcNA had higher gut microbial diversity, higher abundance of potentially beneficial microbes, and lower abundance of potentially pathogenic ones, suggesting alleviation of dysbiosis in mice. EcNI had a higher bacterial richness than CTRL, whereas EcNA had a higher bacterial richness and Shannon index. Notably, compared to CTRL, eight microbial genera with higher abundance in EcNI and EcNA were generally positively correlated with plasma SCFA concentrations and negatively correlated with liver fat droplets and plasma cholesterol concentrations. The other eight microbial genera with lower abundance in EcNI and EcNA were negatively associated with plasma SCFA and positively associated with fat accumulation in the liver and cholesterol in plasma. SCFAs are important bacterial metabolites for maintaining gut health by promoting gut barrier functions.[17] They are also modulators of the MASLD conditions *via* regulating carbohydrate and lipid metabolism.[45] In addition, the intestinal microbiota can metabolize lipids directly, but it can also influence host lipid metabolism by regulating SCFAs, secondary bile acids, and trimethylamine production.[46]

We found higher abundances of several potentially beneficial microbes, including *Eubacterium* J in both EcNI and EcNA, and *Akkermansia* in EcNI than in CTRL. *Eubacterium* is a butyrogenic genus,[47] and several of its species were decreased in individuals with MASLD[48,49] and MASH,[50] and negatively associated with MASLD severity.[51] Although butyric acid was not significantly increased in EcNI and EcNA compared to CTRL, nor was it significantly correlated with *Eubacterium*, *Eubacterium* was negatively correlated with plasma HDL and total cholesterol concentration, and positively correlated with plasma SCFAs, propionic acid and succinic acid. Additionally, *Akkermansia muciniphila* has been shown to improve MASLD in several clinical and rodent studies.[52] Administration of *A. muciniphila* can alleviate MASLD symptoms, including weight gain, insulin resistance, hepatic steatosis, hepatic inflammation, serum triglycerides, and improve gut barrier integrity in high-fat diet (HFD)-fed mice.[53−56] These results indicate that our interventions could elevate these potentially beneficial microbes, which can contribute to MASLD recovery.

On the other hand, there were lower abundances of several potentially detrimental microbes, including *Bacteroides* H in EcNI, and *Faecalibaculum* and *Talaromyces* in EcNA, compared to CTRL. *Bacteroides* H and *Talaromyces* were also negatively correlated with plasma SCFAs, succinic acid and propionic acid, respectively. *Bacteroides* encompasses many species, exhibiting differing phenotypes ranging from commensals to pathogens.[57] Specific *Bacteroides* strains have been shown *in vitro* to potentially alleviate MASLD by enhancing gut barrier functions, exhibiting antimicrobial activity, and reducing lipid accumulation in liver cells, while others may exacerbate MASLD.[58] Various mechanisms for how increased *Bacteroides* abundance can aggravate MASLD have been proposed, including deoxycholic acid-induced hepatic apoptosis and insulin resistance promoted by branched-chain amino acids.[59]

For *Faecalibaculum*, its abundance was higher in the HFD-induced MASLD[60−71] mouse model, positively associated with serum lipid concentration[64] and MASLD-related parameters,[63,65] while treatments that reduced its abundance resulted in lowered hepatic steatosis, oxidative stress, and inflammation.[66,67,70] *Holdemanella biformis*, the human homologue of *Faecalibaculum rodentium*,[72] has also been shown to be enriched in individuals with liver fibrosis.[73] Regarding the fungal gut microbiota, the role of mycobiome dysbiosis in MASLD is poorly understood. There is only one study where *Talaromyces* was found to be higher in individuals with MASLD.[74] Studies have shown changes in intestinal microbiota after treatment with FGF19 and reduction in gut inflammation,[75] while IGF1 can enhance intestinal epithelium cell proliferation[76] and gut barrier function.[77,78] In our study, the beneficial effects of these hormones could produce changes in the gut environment, resulting in a more balanced microbiota composition with increased beneficial microbes, producing beneficial metabolites to exert positive feedback, contributing to MASLD recovery.

The effects of EcNI and EcNA extend from the gut to the liver, and identifying the underlying metabolic pathways and metabolites within the gut-liver axis can help us to understand their roles in promoting balance within the system. EcNA had higher plasma propionate and acetate concentrations than CTRL. Particularly, propionate supplementation has been shown to reduce hepatic steatosis in overweight adults[79] and hepatic triglyceride concentration in mice with HFD-induced obesity.[80] Acetate is also upregulated in various upregulated pathways, including the pyruvate metabolism pathway in the liver that was upregulated in EcNI, the glycolysis or gluconeogenesis pathway in cecum and liver, glyoxylate and dicarboxylate metabolism pathway in the liver, and pyruvate metabolism pathway in the liver and plasma that were upregulated in EcNA, compared to CTRL. These upregulations in acetate-associated metabolic pathways may suggest greater acetate availability to both the host and gut microbes. Notably, our study found that these pathways were negatively correlated to hepatic steatosis, supporting the crosstalk between the gut and liver. Elevated acetate abundance in the gut and colonization of acetate-producing microbes have been associated with reduced hepatic steatosis, fibrosis, and hepatocellular carcinoma in mice and cell lines.[81,82] As recently proposed,[83] there is a shortage of different substrates, including SCFAs, during dysbiosis. In particular, acetate is a key SCFA driving microbial energy metabolism, which enhances mutualistic symbiosis, promotes the growth of many butyrate producers, and suppresses the production of several toxins known to disrupt host metabolism. These findings highlight the beneficial effects of elevated SCFA, mainly acetate, on MASLD recovery, as observed in our study. Interestingly, the hormones IGF1, aldafermin, and SCFA have similar beneficial effects on the gut-liver axis. IGF1, FGF19, and SCFAs improve the gut barrier function by reducing intestinal permeability and upregulating tight junctions, including claudin and occludin.[75−77,84−86] IGF1 and SCFAs can also support intestinal epithelial growth.[87,88] In the liver, IGF1, FGF19, and SCFAs can influence glucose and lipid metabolism and improve insulin sensitivity to reduce hepatic steatosis.[23,89−94] Together, the accelerated MASLD recovery observed in the intervention groups could be explained by hormonal treatment and positive intestinal microbiota changes.

https://doi.org/10.1021/acs.jafc.5c01674
J. Agric. Food Chem. 2025, 73, 15199−15214

Compared to CTRL, EcNA had lower abundances of acetyl-coenzyme A (CoA), despite the overall higher metabolite abundance associated with the glycolysis or gluconeogenesis pathway and the citrate cycle pathway in the liver and cecum. Such downregulation of acetyl-CoA can potentially lower lipid synthesis[95] and subsequently reduce hepatic steatosis, as observed in our study. Acetyl-CoA also enters the superpathway of geranylgeranyldiphosphate biosynthesis in the liver, which was downregulated in EcNA, to produce cholesterol, as shown previously.[31] Downregulation of acetyl-CoA as the starting substrate of cholesterol synthesis[96] and the overall downregulation of the superpathway by EcNA supports the reduction of total, HDL, and LDL cholesterol concentrations in the plasma by EcNA, which was also observed in EcNI. These positive outcomes may be attributed to the effects of the hormonal treatments, where intervention with IGF1 has been shown to inhibit hepatic accumulation of cholesterol in growth hormone-deficient mice[97] and reduce serum cholesterol concentrations[98] while aldafermin reduced hepatic cholesterol concentrations in mice fed an HFD.[93]

In the current study, both EcNI and EcNA downregulated the metabolites in the steroid hormone biosynthesis pathway in the plasma, including cholesterol as the starting substrate for this pathway and the stress hormones corticosterone and cortisol. This is also supported by the reduced abundance of predicted bacterial genes involved in the pathway. Metabolites of this pathway in the plasma and liver were also negatively correlated with hepatic steatosis. Cholesterol accumulation is a well-known cause of liver damage and contributes to MASLD progression.[96] Chronic exposure to corticosterone induces hepatic steatosis in different animal models.[99−102] Cortisol is also a member of the unannotated P-CAG-1, significantly lower in EcNI and EcNA than in CTRL. Both cortisol and P-CAG-1 were positively correlated with liver fat droplets. Hypercortisolism is also associated with the MASLD condition.[18,103] The overall reduction of cholesterol, corticosterone, and cortisol in the downregulated steroid hormone biosynthesis pathway by EcNI and EcNA can potentially support the observed lowered hepatic steatosis.

Oxidative stress is a well-established MASLD promoter.[104] Metabolites associated with the pentose phosphate pathway in the cecum were higher in EcNA than in CTRL. The pentose phosphate pathway can generate nicotinamide adenine dinucleotide phosphate (NADPH)[105] to produce the reduced form of glutathione for lowering oxidative stress and reactive oxygen species.[106,107] This result parallels the downregulation of glutathione and glutathione-associated pathways by EcNA observed in the liver in our previous publication.[31] Even though EcNI had a lower abundance of the metabolites involved in the pentose phosphate pathway in the liver, IGF1 itself has been shown to reduce oxidative damage in the liver.[98] Thus, it may already be enough to mitigate hepatic oxidative stress. Furthermore, the metabolites related to the pyruvate metabolism pathway and the pyruvate metabolite itself were higher in the plasma in EcNA compared to CTRL. Pyruvate, based on its α-keto-carboxylate structure,[108] has also been shown to exhibit antioxidant properties that lower oxidative stress.[109,110] These findings suggest that our interventions help alleviate MASLD by potentially mitigating oxidative damage.

In our study, IGF1 and aldafermin production in our strains was successfully demonstrated *in vitro*, together with their survival and recovery as viable colony-forming units (CFUs) in mouse feces. These results indicate that our strains survive and express these hormones in the gut. However, a limitation of our study was the inability to detect the concentrations of IGF1 and aldafermin in the mice's systemic blood plasma samples. This may be due to the short half-life of FGF19, as mentioned in our previous paper,[31] and/or that the produced IGF1 and aldafermin concentrations fell below the detection limit of our method. Using more sensitive approaches and measurements in the blood from the hepatic portal vein and gut content, closer to the site of hormone expression, may potentially overcome this limitation. Despite this, there was a clear distinction in the outcomes of EcNI and EcNA interventions, especially in the gut microbiota composition. The exact mechanisms by which the interventions influence the gut microbiota are not fully explained, but the produced hormones IGF1 and aldafermin could have changed the intestinal environment and influenced the gut microbiota composition. This interplay between hormonal effects, microbiota changes, and their positive effects on MASLD alleviation should be further investigated.

Advanced microbiome therapeutics (AMTs) using *E. coli* Nissle 1917 strains expressing IGF1 and aldafermin, coupled with dietary changes, effectively boosted MASLD recovery compared with dietary changes alone by lowering hepatic steatosis and plasma cholesterol, while enhancing body weight loss. Our results suggest the following mechanisms behind such improvements: (1) alleviating microbial dysbiosis by increasing bacterial diversity, plasma acetate and propionate, abundances of potentially beneficial bacteria *Eubacterium* J and *Akkermansia* while lowering that of potentially detrimental bacteria *Bacteroides* H and *Faecalibaculum* and fungi *Talaromyces*; and (2) modulating metabolomic profiles by reducing acetyl-CoA, steroid hormone biosynthesis pathway, corticosterone, and cortisol, while elevating pyruvate and pentose phosphate pathway. These changes in the gut microbiota composition and metabolomic profiles suggest an improvement in the gut-liver axis that can potentially support the reduced hepatic steatosis observed. Furthermore, IGF1 and aldafermin production and higher SCFA concentrations have similar beneficial effects that can improve the gut environment and gut-liver axis while accelerating MASLD recovery. These findings indicate that our AMTs are promising candidates for novel treatments for MASLD.[111−132]

■ ASSOCIATED CONTENT

Data Availability Statement

16S and ITS rRNA sequencing data have been deposited at the NCBI GenBank Sequence Read Archive with accession numbers PRJNA1121063 and PRJNA1122398, respectively. Nontargeted metabolomics data have been deposited at the metabolights with accession numbers MTBLS7781. The R codes used for metabolomic data processing and statistical analyses are available online (https://github.com/antonvsdata/notame). All data are available from the corresponding authors upon request.

Supporting Information

The Supporting Information is available free of charge at https://pubs.acs.org/doi/10.1021/acs.jafc.5c01674.

Construction of plasmid (Figure S1); MRI fat index (Figure S2); characterization of *E. coli* Nissle 1917 strains (Figure S3); body weight trends (Figure S4); Spearman's correlation heatmap (Figure S5); KEGG maps (Figures S6−S15); SCFA in plasma and cecum

https://doi.org/10.1021/acs.jafc.5c01674
J. Agric. Food Chem. 2025, 73, 15199−15214

content (Table S1); detailed information on the CAGs (Table S2); methods and materials (PDF)

AUTHOR INFORMATION

Corresponding Authors

Hani El-Nezami − *School of Medicine, Institute of Public Health and Clinical Nutrition, University of Eastern Finland, Kuopio 70210, Finland; School of Biological Sciences, University of Hong Kong, Pokfulam, Hong Kong SAR 999077, China*; Email: hani.el-nezami@uef.fi, elnezami@hku.hk

Carlos Gómez-Gallego − *School of Medicine, Institute of Public Health and Clinical Nutrition, University of Eastern Finland, Kuopio 70210, Finland*; orcid.org/0000-0003-0219-1827; Email: carlos.gomezgallego@uef.fi

Authors

Johnson Lok − *School of Medicine, Institute of Public Health and Clinical Nutrition, University of Eastern Finland, Kuopio 70210, Finland*

Congjia Chen − *School of Biological Sciences, University of Hong Kong, Pokfulam, Hong Kong SAR 999077, China*; orcid.org/0009-0004-6800-3184

Valeria Iannone − *School of Medicine, Institute of Public Health and Clinical Nutrition, University of Eastern Finland, Kuopio 70210, Finland*

Ambrin Farizah Babu − *School of Medicine, Institute of Public Health and Clinical Nutrition, University of Eastern Finland, Kuopio 70210, Finland; Afekta Technologies Ltd., Kuopio 70210, Finland*

Emily Kwun Kwan Lo − *School of Biological Sciences, University of Hong Kong, Pokfulam, Hong Kong SAR 999077, China*

Ruben Vazquez-Uribe − *Technical University of Denmark, The Novo Nordisk Foundation Center for Biosustainability, Kongens Lyngby 2800, Denmark; Vlaams Instituut voor Biotechnologie, Center for Microbiology, Leuven 3001, Belgium*

Troels Holger Vaaben − *Technical University of Denmark, The Novo Nordisk Foundation Center for Biosustainability, Kongens Lyngby 2800, Denmark*

Mikko Kettunen − *Biomedical Imaging Unit, A.I. Virtanen Institute for Molecular Sciences, University of Eastern Finland, Kuopio 70211, Finland*

Otto Savolainen − *School of Medicine, Institute of Public Health and Clinical Nutrition, University of Eastern Finland, Kuopio 70210, Finland; Chalmers Mass Spectrometry Infrastructure, Department of Life Sciences, Chalmers University of Technology, SE-412 96 Gothenburg, Sweden*

Ursula Schwab − *School of Medicine, Institute of Public Health and Clinical Nutrition, University of Eastern Finland, Kuopio 70210, Finland; Department of Medicine, Endocrinology and Clinical Nutrition, Kuopio University Hospital, Kuopio 70210, Finland*

Morten Otto Alexander Sommer − *Technical University of Denmark, The Novo Nordisk Foundation Center for Biosustainability, Kongens Lyngby 2800, Denmark*; orcid.org/0000-0003-4005-5674

Kati Hanhineva − *School of Medicine, Institute of Public Health and Clinical Nutrition, University of Eastern Finland, Kuopio 70210, Finland; Afekta Technologies Ltd., Kuopio 70210, Finland; Department of Life Technologies, Food Sciences Unit, University of Turku, Turku 20014, Finland*

Marjukka Kolehmainen − *School of Medicine, Institute of Public Health and Clinical Nutrition, University of Eastern Finland, Kuopio 70210, Finland*

Complete contact information is available at: https://pubs.acs.org/10.1021/acs.jafc.5c01674

Author Contributions

¶J.L. and C.C. contributed equally to this work and shared first authorship.

Funding

This work was supported by the ITN Marie Curie BestTreat-Building a Gut Microbiome Engineering Toolbox for *In Situ* Therapeutic Treatments for Nonalcoholic Fatty Liver Disease (grant number 813781), The Cell2Eat (Research Council of Finland decision number 339184), the Novo Nordisk Foundation, NNF grant numbers NNF20CC0035580, NNF21OC0070455, and NNF22OC0081058. K.H. is supported by the Academy of Finland (grant no. 321716) and ERA-NET NEURON (grant no. 334814).

Notes

The authors declare the following competing financial interest(s): M.O.A.S., R.V.U., V.I., C.G.G., H.N., J.L., and M. Kolehmainen are inventors on a patent filed by Technical University of Denmark and University of Eastern Finland on Methods for treatment of non-alcoholic fatty liver diseases (nafld) using advanced microbiome therapeutics (Patent number: WO2023208816).

ACKNOWLEDGMENTS

Miia Reponen and Anton Klåvus are thanked for their support with metabolomics analysis. Part of the work was carried out with the support of the Kuopio Biomedical Imaging Unit, University of Eastern Finland, Kuopio, Finland (part of the Finnish Biomedical Imaging Node, EuroBioImaging). The SciLifeLab Metabolomics platform, Swedish National Infrastructure for Biological Mass Spectrometry (BioMS), and Chalmers Mass Spectrometry Infrastructure (CMSI) are acknowledged for their support with the mass spectrometry analysis of small molecules. High-performance computations were performed using research computing facilities offered by Information Technology Services, the University of Hong Kong. The graphical abstract was made using BioRender (BioRender—biorender.com). More details are provided in the Supporting Information.

ABBREVIATIONS

ALIOS:American lifestyle induced obesity syndrome; ASV:amplicon sequence variant; CAG:coabundance group; CFU:colony-forming units; CoA:coenzyme A; FDR:false-discovery rate; FGF:fibroblast growth factor; HDL:high-density lipoprotein; HFD:high-fat diet; IGF1:insulin-like growth factor 1; ITS:internal transcribed spacer; KEGG:Kyoto encyclopedia of genes and genomes; LDL:low-density lipoprotein; MASH:-metabolic dysfunction-associated steatohepatitis; MASLD:metabolic dysfunction-associated steatotic liver disease; MRI:-magnetic resonance imaging; ORO:Oil Red O; PCoA:principal coordinate analysis; rRNA:ribosomal RNA; SCFA:short-chain fatty acid

REFERENCES

(1) Rinella, M. E.; Lazarus, J. V.; Ratziu, V.; Francque, S. M.; Sanyal, A. J.; Kanwal, F.; et al. A multisociety Delphi consensus statement on

new fatty liver disease nomenclature. *Hepatology* **2023**, *78* (6), 1966−1986.
(2) Dhamija, E.; Paul, S. B.; Kedia, S. Non-alcoholic fatty liver disease associated with hepatocellular carcinoma: An increasing concern. *Indian J. Med. Res.* **2019**, *149* (1), 9−17.
(3) Miao, L.; Targher, G.; Byrne, C. D.; Cao, Y.-Y.; Zheng, M.-H. Current status and future trends of the global burden of MASLD. *Trends Endocrinol. Metab.* **2024**, *35* (8), 697−707.
(4) Teng, M. L.; Ng, C. H.; Huang, D. Q.; Chan, K. E.; Tan, D. J.; Lim, W. H.; et al. Global incidence and prevalence of nonalcoholic fatty liver disease. *Clin. Mol. Hepatol.* **2023**, *29*, S32−S42.
(5) Stefano, J. T.; Duarte, S. M. B.; Altikes, R. G. R. L.; Oliveira, C. P. Non-pharmacological management options for MAFLD: a practical guide. *Ther. Adv. Endocrinol. Metab.* **2023**, *14*, No. 20420188231160394.
(6) Koutoukidis, D. A.; Astbury, N. M.; Tudor, K. E.; Morris, E.; Henry, J. A.; Noreik, M.; et al. Association of weight loss interventions with changes in biomarkers of nonalcoholic fatty liver disease: a systematic review and meta-analysis. *JAMA Intern. Med.* **2019**, *179* (9), 1262−1271.
(7) Houttu, V.; Csader, S.; Nieuwdorp, M.; Holleboom, A. G.; Schwab, U. Dietary interventions in patients with non-alcoholic fatty liver disease: a systematic review and meta-analysis. *Front. Nutr.* **2021**, *8*, No. 716783.
(8) Barte, J. C. M.; Ter Bogt, N.; Bogers, R.; Teixeira, P.; Blissmer, B.; Mori, T.; Bemelmans, W. J. E. Maintenance of weight loss after lifestyle interventions for overweight and obesity, a systematic review. *Obes. Rev.* **2010**, *11* (12), 899−906.
(9) Vilar-Gomez, E.; Martinez-Perez, Y.; Calzadilla-Bertot, L.; Torres-Gonzalez, A.; Gra-Oramas, B.; Gonzalez-Fabian, L.; et al. Weight loss through lifestyle modification significantly reduces features of nonalcoholic steatohepatitis. *Gastroenterology* **2015**, *149* (2), 367−78. e5.
(10) Arredouani, A. Effectiveness of Lifestyle Interventions for Nonalcoholic Fatty Liver Disease Treatment. In *Lifestyle-Related Diseases and Metabolic Syndrome*; IntechOpen, 2022.
(11) Evert, A. B.; Franz, M. J. Why weight loss maintenance is difficult. *Diabetes Spectrum* **2017**, *30* (3), 153−156.
(12) Tilg, H.; Adolph, T. E.; Moschen, A. R. Multiple parallel hits hypothesis in nonalcoholic fatty liver disease: revisited after a decade. *Hepatology* **2021**, *73* (2), 833−842.
(13) Benedé-Ubieto, R.; Cubero, F. J.; Nevzorova, Y. A. Breaking the barriers: the role of gut homeostasis in Metabolic-Associated Steatotic Liver Disease (MASLD). *Gut Microbes* **2024**, *16* (1), No. 2331460.
(14) DeGruttola, A. K.; Low, D.; Mizoguchi, A.; Mizoguchi, E. Current understanding of dysbiosis in disease in human and animal models. *Inflammatory Bowel Dis.* **2016**, *22* (5), 1137−1150.
(15) Song, Q.; Zhang, X. The role of gut−liver axis in gut microbiome dysbiosis associated NAFLD and NAFLD-HCC. *Biomedicines* **2022**, *10* (3), No. 524.
(16) Jayachandran, M.; Qu, S. Non-alcoholic fatty liver disease and gut microbial dysbiosis-underlying mechanisms and gut microbiota mediated treatment strategies. *Rev. Endocr. Metab. Disord.* **2023**, *24* (6), 1189−1204.
(17) Ding, Y.; Yanagi, K.; Cheng, C.; Alaniz, R. C.; Lee, K.; Jayaraman, A. Interactions between gut microbiota and non-alcoholic liver disease: The role of microbiota-derived metabolites. *Pharmacol. Res.* **2019**, *141*, 521−529.
(18) Hutchison, A. L.; Tavaglione, F.; Romeo, S.; Charlton, M. Endocrine aspects of metabolic dysfunction associated steatotic liver disease (MASLD): Beyond insulin resistance. *J. Hepatol.* **2023**, *79* (6), 1524−1541.
(19) Marino, L. Jornayvaz FR. Endocrine causes of nonalcoholic fatty liver disease. *World J. Gastroenterol.* **2015**, *21* (39), 11053−11076.
(20) Takahashi, Y. The Role of Growth Hormone and Insulin-Like Growth Factor-I in the Liver. *Int. J. Mol. Sci.* **2017**, *18* (7), No. 1447.
(21) Cristin, L.; Montini, A.; Martinino, A.; Scarano Pereira, J. P.; Giovinazzo, F.; Agnes, S. The Role of Growth Hormone and Insulin Growth Factor 1 in the Development of Non-Alcoholic Steato-Hepatitis: A Systematic Review. *Cells* **2023**, *12* (4), No. 517.
(22) Adamek, A.; Kasprzak, A. Insulin-like growth factor (IGF) system in liver diseases. *Int. J. Mol. Sci.* **2018**, *19* (5), No. 1308.
(23) Nishizawa, H.; Iguchi, G.; Fukuoka, H.; Takahashi, M.; Suda, K.; Bando, H.; et al. IGF-I induces senescence of hepatic stellate cells and limits fibrosis in a p53-dependent manner. *Sci. Rep.* **2016**, *6* (1), No. 34605.
(24) Tian, H.; Zhang, S.; Liu, Y.; Wu, Y.; Zhang, D. Fibroblast Growth Factors for Nonalcoholic Fatty Liver Disease: Opportunities and Challenges. *Int. J. Mol. Sci.* **2023**, *24* (5), No. 4583.
(25) Jansen, P. L. Fibroblast growth factor 19, a double-edged sword. *Hepatic Oncol.* **2017**, *4* (1), 1−4.
(26) Harrison, S. A.; Neff, G.; Guy, C. D.; Bashir, M. R.; Paredes, A. H.; Frias, J. P.; et al. Efficacy and safety of aldafermin, an engineered FGF19 analog, in a randomized, double-blind, placebo-controlled trial of patients with nonalcoholic steatohepatitis. *Gastroenterology* **2021**, *160* (1), 219−231.e1.
(27) Vazquez-Uribe, R.; Hedin, K. A.; Licht, T. R.; Nieuwdorp, M.; Sommer, M. O. Advanced microbiome therapeutics as a novel modality for oral delivery of peptides to manage metabolic diseases. *Trends Endocrinol. Metab.* **2025**, *36* (1), 29−41.
(28) Vaaben, T. H.; Vazquez-Uribe, R.; Sommer, M. O. A. Characterization of eight bacterial biosensors for microbial diagnostic and therapeutic applications. *ACS Synth. Biol.* **2022**, *11* (12), 4184−4192.
(29) Lynch, J. P.; Goers, L.; Lesser, C. F. Emerging strategies for engineering *Escherichia coli* Nissle 1917-based therapeutics. *Trends Pharmacol. Sci.* **2022**, *43* (9), 772−786.
(30) Zhao, Z.; Xu, S.; Zhang, W.; Wu, D.; Yang, G. Probiotic *Escherichia coli* NISSLE 1917 for inflammatory bowel disease applications. *Food Funct.* **2022**, *13* (11), 5914−5924.
(31) Iannone, V.; Babu, A. F.; Lok, J.; Gómez-Gallego, C.; D'Auria, G.; Vazquez-Uribe, R.; et al. Changes in liver metabolic pathways demonstrate efficacy of the combined dietary and microbial therapeutic intervention in MASLD mouse model. *Mol. Metab.* **2023**, *78*, No. 101823.
(32) Zhang, L. Method for voluntary oral administration of drugs in mice. *STAR Protoc.* **2021**, *2* (1), No. 100330.
(33) Percie du Sert, N.; Hurst, V.; Ahluwalia, A.; Alam, S.; Avey, M.; Baker, M.; et al. The ARRIVE guidelines 2.0: Updated guidelines for reporting animal research. *PLoS Biol.* **2020**, *18* (7), No. e3000410.
(34) Faul, F.; Erdfelder, E.; Buchner, A.; Lang, A. G. Statistical power analyses using G*Power 3.1: tests for correlation and regression analyses. *Behav. Res. Methods* **2009**, *41* (4), 1149−1160.
(35) Lee, H. Y.; Park, J. H.; Seok, S. H.; Baek, M. W.; Kim, D. J.; Lee, K. E.; et al. Human originated bacteria, Lactobacillus rhamnosus PL60, produce conjugated linoleic acid and show anti-obesity effects in diet-induced obese mice. *Biochim. Biophys. Acta, Mol. Cell Biol. Lipids* **2006**, *1761* (7), 736−744.
(36) Iannone, V.; Lok, J.; Babu, A. F.; Gómez-Gallego, C.; Willman, R. M.; Koistinen, V. M.; et al. Associations of altered hepatic gene expression in American lifestyle-induced obesity syndrome diet-fed mice with metabolic changes during NAFLD development and progression. *J. Nutr. Biochem.* **2023**, *115*, No. 109307.
(37) Tetri, L. H.; Basaranoglu, M.; Brunt, E. M.; Yerian, L. M.; Neuschwander-Tetri, B. A. Severe NAFLD with hepatic necroinflammatory changes in mice fed trans fats and a high-fructose corn syrup equivalent. *Am. J. Physiol. Gastrointest. Liver Physiol.* **2008**, *295* (5), G987−G995.
(38) Kamzolas, I.; Vacca, M.; Mørch Harder, L.; Rodriguez-Cuenca, S.; Tiniakos, L.; Perfield, J.; et al. An unbiased ranking of murine dietary models based on their proximity to human Metabolic Dysfunction−associated Steatotic Liver Disease (MASLD). *Nature* **2024**, *6* (6), 1178−1196.
(39) Carper, D.; Coué, M.; Laurens, C.; Langin, D.; Moro, C. Reappraisal of the optimal fasting time for insulin tolerance tests in mice. *Mol. Metab.* **2020**, *42*, No. 101058.

(40) Fristedt, R.; Ruppert, V.; Trower, T.; Cooney, J.; Landberg, R. Quantitation of circulating short-chain fatty acids in small volume blood samples from animals and humans. *Talanta* **2024**, *272*, No. 125743.
(41) Arganda-Carreras, I.; Kaynig, V.; Rueden, C.; Eliceiri, K. W.; Schindelin, J.; Cardona, A.; Seung, H. S. Trainable Weka Segmentation: a machine learning tool for microscopy pixel classification. *Bioinformatics* **2017**, *33* (15), 2424−2426.
(42) Klåvus, A.; Kokla, M.; Noerman, S.; Koistinen, V. M.; Tuomainen, M.; Zarei, I.; et al. "Notame": Workflow for Non-Targeted LC−MS Metabolic Profiling. *Metabolites* **2020**, *10* (4), No. 135.
(43) R Core Team. *R: A language and Environment for Statistical Computing*; R Foundation for Statistical Computing: Vienna, Austria, 2022.
(44) Iannone, V.; Vaittinen, M.; Gómez-Gallego, C.; Mikkonen, S.; Lok, J.; D'Auria, G.; et al. The effect of aldafermin expressing-*Escherichia coli* Nissle 1917 along with dietary change on visceral adipose tissue in MASLD mouse model. *Int. J. Obes.* **2025**, 1−11.
(45) Zhou, D.; Fan, J. G. Microbial metabolites in non-alcoholic fatty liver disease. *World J. Gastroenterol.* **2019**, *25* (17), 2019−2028.
(46) Schoeler, M.; Caesar, R. Dietary lipids, gut microbiota and lipid metabolism. *Rev. Endocr. Metab. Disord.* **2019**, *20*, 461−472.
(47) Singh, V.; Lee, G.; Son, H.; Koh, H.; Kim, E. S.; Unno, T.; Shin, J. H. Butyrate producers,"The Sentinel of Gut": Their intestinal significance with and beyond butyrate, and prospective use as microbial therapeutics. *Front. Microbiol.* **2023**, *13*, No. 1103836.
(48) Aron-Wisnewsky, J.; Vigliotti, C.; Witjes, J.; Le, P.; Holleboom, A. G.; Verheij, J.; et al. Gut microbiota and human NAFLD: disentangling microbial signatures from metabolic disorders. *Nat. Rev. Gastroenterol. Hepatol.* **2020**, *17* (5), 279−297.
(49) Yu, J.; Zhang, H.; Chen, L.; Ruan, Y.; Chen, Y.; Liu, Q. Disease-associated gut microbiota reduces the profile of secondary bile acids in pediatric nonalcoholic fatty liver disease. *Front. Cell. Infect. Microbiol.* **2021**, *11*, No. 698852.
(50) Zhu, L.; Baker, S. S.; Gill, C.; Liu, W.; Alkhouri, R.; Baker, R. D.; Gill, S. R. Characterization of gut microbiomes in nonalcoholic steatohepatitis (NASH) patients: a connection between endogenous alcohol and NASH. *Hepatology* **2013**, *57* (2), 601−609.
(51) Oh, T. G.; Kim, S. M.; Caussy, C.; Fu, T.; Guo, J.; Bassirian, S.; et al. A universal gut-microbiome-derived signature predicts cirrhosis. *Cell Metab.* **2020**, *32* (5), 878−88.e6.
(52) Han, Y.; Li, L.; Wang, B. Role of Akkermansia muciniphila in the development of nonalcoholic fatty liver disease: current knowledge and perspectives. *Front. Med.* **2022**, *16* (5), 667−685.
(53) Nian, F.; Wu, L.; Xia, Q.; Tian, P.; Ding, C.; Lu, X. Akkermansia muciniphila and bifidobacterium bifidum prevent nafld by regulating fxr expression and gut microbiota. *J. Clin. Transl. Hepatol.* **2023**, *11* (4), 763−776.
(54) Kim, S.; Lee, Y.; Kim, Y.; Seo, Y.; Lee, H.; Ha, J.; et al. Akkermansia muciniphila prevents fatty liver disease, decreases serum triglycerides, and maintains gut homeostasis. *Appl. Environ. Microbiol.* **2020**, *86* (7), No. e03004-19.
(55) Rao, Y.; Kuang, Z.; Li, C.; Guo, S.; Xu, Y.; Zhao, D.; et al. Gut Akkermansia muciniphila ameliorates metabolic dysfunction-associated fatty liver disease by regulating the metabolism of L-aspartate via gut-liver axis. *Gut microbes* **2021**, *13* (1), No. 1927633.
(56) Wu, W.; Kaicen, W.; Bian, X.; Yang, L.; Ding, S.; Li, Y.; et al. Akkermansia muciniphila alleviates high-fat-diet-related metabolic-associated fatty liver disease by modulating gut microbiota and bile acids. *Microb. Biotechnol.* **2023**, *16* (10), 1924−1939.
(57) Wexler, H. M. Bacteroides: the good, the bad, and the nitty-gritty. *Clin. Microbiol. Rev.* **2007**, *20* (4), 593−621.
(58) Garcia-Morena, D.; Fernandez-Cantos, M. V.; Escalera, S. L.; Lok, J.; Iannone, V.; Cancellieri, P.; et al. In Vitro Influence of Specific Bacteroidales Strains on Gut and Liver Health Related to Metabolic Dysfunction-Associated Fatty Liver Disease. *Probiotics Antimicrob. Proteins* **2024**, 1498−1512.
(59) Boursier, J.; Mueller, O.; Barret, M.; Machado, M.; Fizanne, L.; Araujo-Perez, F.; et al. The severity of nonalcoholic fatty liver disease is associated with gut dysbiosis and shift in the metabolic function of the gut microbiota. *Hepatology* **2016**, *63* (3), 764−775.
(60) Liu, L.; Fu, Q.; Li, T.; Shao, K.; Zhu, X.; Cong, Y.; Zhao, X. Gut microbiota and butyrate contribute to nonalcoholic fatty liver disease in premenopause due to estrogen deficiency. *PLoS One* **2022**, *17* (2), No. e0262855.
(61) Yan, G.; He, L.; Yu, Z.; Tang, Y.; Yu, S.; Gu, C.; et al. Characteristics of intestinal microbiota in C57BL/6 mice with non-alcoholic fatty liver induced by high-fat diet. *Front. Microbiol.* **2022**, *13*, No. 1051200.
(62) Gu, C.; Zhou, Z.; Yu, Z.; He, M.; He, L.; Luo, Z.; et al. The microbiota and it's correlation with metabolites in the gut of mice with nonalcoholic fatty liver disease. *Front. Cell. Infect. Microbiol.* **2022**, *12*, No. 870785.
(63) Yu, J.; Sun, H.; Yang, Y.; Yan, Y. Sesamolin alleviates nonalcoholic fatty liver disease through modulating gut microbiota and metabolites in high-fat and high-fructose diet-fed mice. *Int. J. Mol. Sci.* **2022**, *23* (22), No. 13853.
(64) Mu, H.; Zhou, Q.; Yang, R.; Zeng, J.; Li, X.; Zhang, R.; et al. Naringin attenuates high fat diet induced non-alcoholic fatty liver disease and gut bacterial dysbiosis in mice. *Front. Microbiol.* **2020**, *11*, No. 585066.
(65) Luo, X.; Zhang, B.; Tan, R.; Gong, P.; et al. Phyllanthus emblica aqueous extract retards hepatic steatosis and fibrosis in NAFLD mice in association with the reshaping of intestinal microecology. *Front. Pharmacol.* **2022**, *13*, No. 893561.
(66) Hu, W.; Gao, W.; Liu, Z.; Fang, Z.; Wang, H.; Zhao, J.; et al. Specific strains of faecalibacterium prausnitzii ameliorate nonalcoholic fatty liver disease in mice in association with gut microbiota regulation. *Nutrients* **2022**, *14* (14), No. 2945.
(67) Duan, R.; Huang, K.; Guan, X.; Li, S.; Shen, M.; Sun, Z.; et al. Tectorigenin ameliorated high-fat diet-induced nonalcoholic fatty liver disease through anti-inflammation and modulating gut microbiota in mice. *Food Chem. Toxicol.* **2022**, *164*, No. 112948.
(68) Wu, X.; Huang, H.; Li, M.; Wang, Y.; Wu, X.; Wang, Q.; et al. Excessive consumption of the sugar rich longan fruit promoted the development of nonalcoholic fatty liver disease via mediating gut dysbiosis. *Food Front.* **2023**, *4* (1), 491−510.
(69) Zhou, Y.; Tian, S.; Qian, L.; Jiang, S.; Tang, Y.; Han, T. DHA-enriched phosphatidylserine ameliorates non-alcoholic fatty liver disease and intestinal dysbacteriosis in mice induced by a high-fat diet. *Food Funct.* **2021**, *12* (9), 4021−4033.
(70) Qian, L.; Tian, S.; Jiang, S.; Tang, Y.; Han, T. DHA-enriched phosphatidylcholine from Clupea harengus roes regulates the gut−liver axis to ameliorate high-fat diet-induced non-alcoholic fatty liver disease. *Food Funct* **2022**, *13* (22), 11555−11567.
(71) Li, C.; Cui, L.; Wang, X.; Yan, Z.; Wang, S.; Zheng, Y. Using intestinal flora to distinguish non-alcoholic steatohepatitis from non-alcoholic fatty liver. *J. Int. Med. Res.* **2020**, *48* (12), No. 0300060520978122.
(72) Zagato, E.; Pozzi, C.; Bertocchi, A.; Schioppa, T.; Saccheri, F.; Guglietta, S.; et al. Endogenous murine microbiota member Faecalibaculum rodentium and its human homologue protect from intestinal tumour growth. *Nat. Microbiol.* **2020**, *5* (3), 511−524.
(73) Kwan, S. Y.; Jiao, J.; Joon, A.; Wei, P.; Petty, L. E.; Below, J. E.; et al. Gut microbiome features associated with liver fibrosis in Hispanics, a population at high risk for fatty liver disease. *Hepatology* **2022**, *75* (4), 955−967.
(74) You, N.; Xu, J.; Wang, L.; Zhuo, L.; Zhou, J.; Song, Y.; et al. Fecal fungi dysbiosis in nonalcoholic fatty liver disease. *Obesity* **2021**, *29* (2), 350−358.
(75) Gadaleta, R. M.; Garcia-Irigoyen, O.; Cariello, M.; Scialpi, N.; Peres, C.; Vetrano, S.; et al. Fibroblast Growth Factor 19 modulates intestinal microbiota and inflammation in presence of Farnesoid X Receptor. *EBioMedicine* **2020**, *54*, No. 102719.
(76) Zheng, Y.; Song, Y.; Han, Q.; Liu, W.; Xu, J.; Yu, Z.; et al. Intestinal epithelial cell-specific IGF1 promotes the expansion of

intestinal stem cells during epithelial regeneration and functions on the intestinal immune homeostasis. *Am. J. Physiol.: Endocrinol. Metab.* **2018**, *315* (4), E638−E649.
(77) Lorenzo-Zuñiga, V.; Rodriguez-Ortigosa, C. M.; Bartoli, R.; Martinez-Chantar, M. L.; Martinez-Peralta, L.; Pardo, A.; et al. Insulin-like growth factor I improves intestinal barrier function in cirrhotic rats. *Gut* **2006**, *55* (9), 1306−1312.
(78) Corpeleijn, W. E.; van Vliet, I.; de Gast-Bakker, D.-A.; van der Schoor, S. R.; Alles, M. S.; Hoijer, M.; et al. Effect of enteral IGF-1 supplementation on feeding tolerance, growth, and gut permeability in enterally fed premature neonates. *J. Pediatr. Gastroenterol. Nutr.* **2008**, *46* (2), 184−190.
(79) Chambers, E. S.; Viardot, A.; Psichas, A.; Morrison, D. J.; Murphy, K. G.; Zac-Varghese, S. E.; et al. Effects of targeted delivery of propionate to the human colon on appetite regulation, body weight maintenance and adiposity in overweight adults. *Gut* **2015**, *64* (11), 1744−1754.
(80) Weitkunat, K.; Schumann, S.; Nickel, D.; Kappo, K. A.; Petzke, K. J.; Kipp, A. P.; et al. Importance of propionate for the repression of hepatic lipogenesis and improvement of insulin sensitivity in high-fat diet-induced obesity. *Mol. Nutr. Food Res.* **2016**, *60* (12), 2611−2621.
(81) Aoki, R.; Onuki, M.; Hattori, K.; Ito, M.; Yamada, T.; Kamikado, K.; et al. Commensal microbe-derived acetate suppresses NAFLD/NASH development via hepatic FFAR2 signalling in mice. *Microbiome* **2021**, *9*, No. 188.
(82) Song, Q.; Zhang, X.; Liu, W.; Wei, H.; Liang, W.; Zhou, Y.; et al. Bifidobacterium pseudolongum-generated acetate suppresses non-alcoholic fatty liver disease-associated hepatocellular carcinoma. *J. Hepatol.* **2023**, *79* (6), 1352−1365.
(83) Daisley, B. A.; Koenig, D.; Engelbrecht, K.; Doney, L.; Hards, K.; Al, K. F.; et al. Emerging connections between gut microbiome bioenergetics and chronic metabolic diseases. *Cell Rep.* **2021**, *37* (10), No. 110087.
(84) Zhao, T.-Y.; Su, L.-P.; Ma, C.-Y.; Zhai, X.-H.; Duan, Z.-J.; Zhu, Y.; et al. IGF-1 decreases portal vein endotoxin via regulating intestinal tight junctions and plays a role in attenuating portal hypertension of cirrhotic rats. *BMC Gastroenterol.* **2015**, *15*, No. 77.
(85) Pohl, K.; Moodley, P.; Dhanda, A. The effect of increasing intestinal short-chain fatty acid concentration on gut permeability and liver injury in the context of liver disease: A systematic review. *J. Gastroenterol. Hepatol.* **2022**, *37* (8), 1498−1506.
(86) Saleri, R.; Borghetti, P.; Ravanetti, F.; Cavalli, V.; Ferrari, L.; De Angelis, E.; et al. Effects of different short-chain fatty acids (SCFA) on gene expression of proteins involved in barrier function in IPEC-J2. *Porcine Health Manage.* **2022**, *8* (1), No. 21.
(87) Bohin, N.; McGowan, K. P.; Keeley, T. M.; Carlson, E. A.; Yan, K. S.; Samuelson, L. C. Insulin-like growth factor-1 and mTORC1 signaling promote the intestinal regenerative response after irradiation injury. *Cell. Mol. Gastroenterol. Hepatol.* **2020**, *10* (4), 797−810.
(88) Venegas, D. P.; De la Fuente, M. K.; Landskron, G.; Gonzalez, M. J.; Quera, R.; Dijkstra, G.; et al. Short Chain Fatty Acids (SCFAs)-Mediated Gut Epithelial and Immune Regulation and Its Relevance for Inflammatory Bowel Diseases. *Front. Immunol.* **2019**, *10*, No. 277.
(89) Liu, Z.; Cordoba-Chacon, J.; Kineman, R. D.; Cronstein, B. N.; Muzumdar, R.; Gong, Z.; et al. Growth hormone control of hepatic lipid metabolism. *Diabetes* **2016**, *65* (12), 3598−3609.
(90) De Ita, J. R.; Castilla-Cortázar, I.; Aguirre, G.; Sánchez-Yago, C.; Santos-Ruiz, M. O.; Guerra-Menéndez, L.; et al. Altered liver expression of genes involved in lipid and glucose metabolism in mice with partial IGF-1 deficiency: an experimental approach to metabolic syndrome. *J. Transl. Med.* **2015**, *13*, No. 13.
(91) Zhou, H.; Yu, B.; Sun, J.; Liu, Z.; Chen, H.; Ge, L.; Chen, D. Short-chain fatty acids can improve lipid and glucose metabolism independently of the pig gut microbiota. *J. Anim. Sci. Biotechnol.* **2021**, *12*, No. 12.
(92) Den Besten, G.; Bleeker, A.; Gerding, A.; van Eunen, K.; Havinga, R.; van Dijk, T. H.; et al. Short-chain fatty acids protect against high-fat diet−induced obesity via a PPARγ-dependent switch from lipogenesis to fat oxidation. *Diabetes* **2015**, *64* (7), 2398−2408.
(93) Zhou, M.; Learned, R. M.; Rossi, S. J.; DePaoli, A. M.; Tian, H.; Ling, L. Engineered FGF19 eliminates bile acid toxicity and lipotoxicity leading to resolution of steatohepatitis and fibrosis in mice. *Hepatol. Commun.* **2017**, *1* (10), 1024−1042.
(94) Dolegowska, K.; Marchelek-Mysliwiec, M.; Nowosiad-Magda, M.; Slawinski, M.; Dolegowska, B. FGF19 subfamily members: FGF19 and FGF21. *J. Physiol. Biochem.* **2019**, *75*, 229−240.
(95) Pietrocola, F.; Galluzzi, L.; Bravo-San Pedro, J. M.; Madeo, F.; Kroemer, G. Acetyl coenzyme A: a central metabolite and second messenger. *Cell Metab.* **2015**, *21* (6), 805−821.
(96) Malhotra, P.; Gill, R. K.; Saksena, S.; Alrefai, W. A. Disturbances in cholesterol homeostasis and non-alcoholic fatty liver diseases. *Front. Med.* **2020**, *7*, No. 467.
(97) Fukunaga, K.; Imachi, H.; Lyu, J.; Dong, T.; Sato, S.; Ibata, T.; et al. IGF1 suppresses cholesterol accumulation in the liver of growth hormone-deficient mice via the activation of ABCA1. *Am. J. Physiol.-Endocrinol. Metab.* **2018**, *315* (6), E1232−E1241.
(98) Garcia-Fernandez, M.; Delgado, G.; Puche, J. E.; González-Barón, S.; Castilla Cortázar, I. Low doses of insulin-like growth factor I improve insulin resistance, lipid metabolism, and oxidative damage in aging rats. *Endocrinology* **2008**, *149* (5), 2433−2442.
(99) Hu, Y.; Sun, Q.; Hu, Y.; Hou, Z.; Zong, Y.; Omer, N. A.; et al. Corticosterone-induced lipogenesis activation and lipophagy inhibition in chicken liver are alleviated by maternal betaine supplementation. *J. Nutr.* **2018**, *148* (3), 316−325.
(100) Lin, H.; Sui, S.; Jiao, H.; Buyse, J.; Decuypere, E. Impaired development of broiler chickens by stress mimicked by corticosterone exposure. *Comp. Biochem. Physiol., Part A:Mol. Integr. Physiol.* **2006**, *143* (3), 400−405.
(101) D'souza, A. M.; Beaudry, J. L.; Szigiato, A. A.; Trumble, S. J.; Snook, L. A.; Bonen, A.; et al. Consumption of a high-fat diet rapidly exacerbates the development of fatty liver disease that occurs with chronically elevated glucocorticoids. *Am. J. Physiol.: Gastrointest. Liver Physiol.* **2012**, *302* (8), G850−G863.
(102) Allard, J.; Le Guillou, D.; Begriche, K.; Fromenty, B. Drug-induced liver injury in obesity and nonalcoholic fatty liver disease. *Adv. Pharmacol.* **2019**, *85*, 75−107.
(103) Polyzos, S. A.; Targher, G. Role of glucocorticoids in metabolic dysfunction-associated steatotic liver disease. *Curr. Obes. Rep.* **2024**, *13*, 242−255.
(104) Chen, Z.; Tian, R.; She, Z.; Cai, J.; Li, H. Role of oxidative stress in the pathogenesis of nonalcoholic fatty liver disease. *Free Radical Biol. Med.* **2020**, *152*, 116−141.
(105) Stincone, A.; Prigione, A.; Cramer, T.; Wamelink, M. M.; Campbell, K.; Cheung, E.; et al. The return of metabolism: biochemistry and physiology of the pentose phosphate pathway. *Biol. Rev.* **2015**, *90* (3), 927−963.
(106) Ponomareva, D.; Ivanov, A.; Bregestovski, P. Analysis of the Effects of Pentose Phosphate Pathway Inhibition on the Generation of Reactive Oxygen Species and Epileptiform Activity in Hippocampal Slices. *Int. J. Mol. Sci.* **2024**, *25* (3), No. 1934.
(107) Tang, B. L. Neuroprotection by glucose-6-phosphate dehydrogenase and the pentose phosphate pathway. *J. Cell. Biochem.* **2019**, *120* (9), 14285−14295.
(108) Mallet, R. T.; Sun, J.; Knott, E. M.; Sharma, A. B.; Olivencia-Yurvati, A. H. Metabolic cardioprotection by pyruvate: recent progress. *Exp. Biol. Med.* **2005**, *230* (7), 435−443.
(109) Wang, X.; Perez, E.; Liu, R.; Yan, L.-J.; Mallet, R. T.; Yang, S.-H. Pyruvate protects mitochondria from oxidative stress in human neuroblastoma SK-N-SH cells. *Brain Res.* **2007**, *1132*, 1−9.
(110) Das, U. N. Pyruvate is an endogenous anti-inflammatory and anti-oxidant molecule. *Med. Sci. Monit.: Int. Med. J. Exp. Clin. Res.* **2006**, *12* (5), RA79−RA84.
(111) Armetta, J.; Schantz-Klausen, M.; Shepelin, D.; Vazquez-Uribe, R.; Bahl, M. I.; Laursen, M. F.; et al. *Escherichia coli* promoters with consistent expression throughout the murine gut. *ACS Synth. Biol.* **2021**, *10* (12), 3359−3368.
(112) Bolyen, E.; Rideout, J. R.; Dillon, M. R.; Bokulich, N. A.; Abnet, C. C.; Al-Ghalith, G. A.; et al. Reproducible, interactive,

scalable and extensible microbiome data science using QIIME 2. *Nat. Biotechnol.* **2019**, *37* (8), 852−857.
(113) Martin, M. Cutadapt removes adapter sequences from high-throughput sequencing reads. *EMBnet J.* **2011**, *17* (1), 10−12.
(114) Callahan, B. J.; McMurdie, P. J.; Rosen, M. J.; Han, A. W.; Johnson, A. J. A.; Holmes, S. P. DADA2: High-resolution sample inference from Illumina amplicon data. *Nat. Methods* **2016**, *13* (7), 581−583.
(115) Bokulich, N. A.; Kaehler, B. D.; Rideout, J. R.; Dillon, M.; Bolyen, E.; Knight, R.; et al. Optimizing taxonomic classification of marker-gene amplicon sequences with QIIME 2's q2-feature-classifier plugin. *Microbiome* **2018**, *6* (1), 1−17.
(116) McDonald, D.; Jiang, Y.; Balaban, M.; Cantrell, K.; Zhu, Q.; Gonzalez, A.; et al. Greengenes2 unifies microbial data in a single reference tree. *Nat. Biotechnol.* **2023**, *42*, 715−718.
(117) Nilsson, R. H.; Larsson, K.-H.; Taylor, A. F. S.; Bengtsson-Palme, J.; Jeppesen, T. S.; Schigel, D.; et al. The UNITE database for molecular identification of fungi: handling dark taxa and parallel taxonomic classifications. *Nucleic Acids Res.* **2019**, *47* (D1), D259−D264.
(118) McMurdie, P. J.; Holmes, S. phyloseq: an R package for reproducible interactive analysis and graphics of microbiome census data. *PLoS One* **2013**, *8* (4), No. e61217.
(119) Oksanen, J.; Simpson, G. L.; Blanchet, F. G.; Kindt, R.; Legendre, P.; Minchin, P. R.et al. *Vegan: Community Ecology Package, 2.6−2*; R Foundation for Statistical Computing: Vienna (Austria), 2022.
(120) Douglas, G. M.; Maffei, V. J.; Zaneveld, J. R.; Yurgel, S. N.; Brown, J. R.; Taylor, C. M.; et al. PICRUSt2 for prediction of metagenome functions. *Nat. Biotechnol.* **2020**, *38* (6), 685−688.
(121) Kanehisa, M.; Furumichi, M.; Sato, Y.; Kawashima, M.; Ishiguro-Watanabe, M. KEGG for taxonomy-based analysis of pathways and genomes. *Nucleic Acids Res.* **2023**, *51* (D1), D587−D92.
(122) Tsugawa, H.; Cajka, T.; Kind, T.; Ma, Y.; Higgins, B.; Ikeda, K.; et al. MS-DIAL: data-independent MS/MS deconvolution for comprehensive metabolome analysis. *Nat. Methods* **2015**, *12* (6), 523−526.
(123) Pang, Z.; Chong, J.; Zhou, G.; de Lima Morais, D. A.; Chang, L.; Barrette, M.; et al. MetaboAnalyst 5.0: narrowing the gap between raw spectra and functional insights. *Nucleic Acids Res.* **2021**, *49* (W1), W388−W96.
(124) Li, S.; Park, Y.; Duraisingham, S.; Strobel, F. H.; Khan, N.; Soltow, Q. A.; et al. Predicting network activity from high throughput metabolomics. *PLoS Comput. Biol.* **2013**, *9* (7), No. e1003123.
(125) Subramanian, A.; Tamayo, P.; Mootha, V. K.; Mukherjee, S.; Ebert, B. L.; Gillette, M. A.; et al. Gene set enrichment analysis: a knowledge-based approach for interpreting genome-wide expression profiles. *Proc. Natl. Acad. Sci. U.S.A.* **2005**, *102* (43), 15545−15550.
(126) Korotkevich, G.; Sukhov, V.; Sergushichev, A. Fast gene set enrichment analysis *BioRxiv* 2019.
(127) Luo, W.; Brouwer, C. Pathview: an R/Bioconductor package for pathway-based data integration and visualization. *Bioinformatics* **2013**, *29* (14), 1830−1831.
(128) Langfelder, P.; Horvath, S. WGCNA: an R package for weighted correlation network analysis. *BMC Bioinf.* **2008**, *9* (1), 1−13.
(129) Lin, H.; Peddada, S. D. Analysis of compositions of microbiomes with bias correction. *Nat. Commun.* **2020**, *11* (1), No. 3514.
(130) Segata, N.; Izard, J.; Waldron, L.; Gevers, D.; Miropolsky, L.; Garrett, W. S.; Huttenhower, C. Metagenomic biomarker discovery and explanation. *Genome Biol.* **2011**, *12*, No. R60.
(131) Nearing, J. T.; Douglas, G. M.; Hayes, M. G.; MacDonald, J.; Desai, D. K.; Allward, N.; et al. Microbiome differential abundance methods produce different results across 38 datasets. *Nat. Commun.* **2022**, *13* (1), No. 342.
(132) Kim, S. ppcor: an R package for a fast calculation to semi-partial correlation coefficients. *Commun. Stat. Appl. Methods* **2015**, *22* (6), 665−674.

https://doi.org/10.1021/acs.jafc.5c01674
J. Agric. Food Chem. 2025, 73, 15199−15214